Application of The Spectral Element Method to Buoyancy Driven Flows

A Thesis Submitted
in Partial Fulfilment of the Requirements
for the Degree of

MASTER OF TECHNOLOGY

by

SATYA PRAKASH

to the
Department of Mechanical Engineering
INDIAN INSTITUTE OF TECHNOLOGY
KANPUR
April, 1995

To
my Mother

CERTIFICATE

This is to certify that the present work entitled **Application of The Spectral Element Method to Buoyancy Driven Flows** *was carried out by* **Satya Prakash** *under our supervision and it has not been submitted elsewhere for a degree.*

Dr. V. Eswaran
Department of Mech. Engg.
Indian Institute of Technology
Kanpur

Dr. G. Biswas
Department of Mech. Engg.
Indian Institute of Technology
Kanpur

April, 1995

ABSTRACT

The stream function, vorticity form of momentum equations together with the equation for conservation of energy are solved numerically using the Spectral Element Method for two and three dimensional natural convective flows. For the two dimensional situation, two physical problems, such as, flow and heat transfer in a buoyancy driven cavity and natural convection in a closed cavity with discrete heat sources have been considered. For the three dimensional situation, computations have been performed for natural convection heat transfer from rectangular vertical fin arrays. The streamlines, the vorticity distribution, and the temperature fields for various values of Rayleigh and Prandtl numbers are obtained. Subsequently, the influence of different geometrical parameters, Rayleigh and Prandtl numbers on the flow and heat transfer is investigated. An attempt has been undertaken to compare the predicted results with the results reported in open literature by other investigators.

The above said problems find applications in cooling of electronic equipments and integrated circuit packages.

ACKNOWLEDGEMENTS

I take this opportunity to express my deep gratitude, whole hearted regards and sincere thanks to my thesis supervisors Dr. V. Eswaran and Dr. Gautam Biswas for rendering their valuable knowledge, excellent guidance, allround support and encouragement. I shall always remain obliged to their greatness in showing deep interest to help me complete my work.

I am thankful to Mr. Subbarao, Mr. Atul, Sumitesh, Pulak and Arun for helping me in this work. Also, acknowledgements are due to many other friends who made my stay at IIT Kanpur a memorable one.

My special thanks are also due to Mr. K. S. Yadav who gave me healthy cooperation and boosted my morale for my work.

I express my sincere gratitude to my family members who have been a constant source of inspiration and encouragement throughout the course of this work. Without their cooperation, the present work would have been an impossibility.

- SATYA PRAKASH

Contents

List of Tables

List of Figures

NOMENCLATURE

a,b	Elemental location
Ar	Aspect ratio
$[C^i]$, [C]	Elemental left side coefficient matrix
$\{e^i\}$, {e}	Elemental right side coefficient matrix
e_x	Number of elements in x direction
e_y	Number of elements in y direction
f	Forcing function in Helmholtz equation
{ f }	Array of forcing function at the grid points
g	Acceleration due to gravity
Gr	Grashof number
H	Height of the cavity
I	functional
L	Length of cavity
N_x	Number of Gauss-Lobatto Chebyshev points in x direction
N_y	Number of Gauss-Lobatto Chebyshev points in y direction
Nu	Nusselt number
p	Pressure
P	Nondimensional pressure
Pr	Prandtl number
Ra	Rayleigh number
t	time
T	Temperature
u,v	Velocity components
U,V	Nondimensional velocity components
x,y,z	Cartesian coordinates
X,Y,Z	Nondimensional cartesian coordinates

Greek symbols

α	Thermal diffusivity
β	Cofficient of volumetric expasion
Γ	Diffusion coefficient
θ	Non dimensional temperature
λ	Dummy parameter
Λ	A constant in general transport equation
ρ	Density
ν	Kinematic viscosity
τ	Non dimensional time
$\Delta\tau$	Non dimensional time step
ϕ	Unknown function in general transport equation
ψ	Stream function
ω	Vorticity
∇	Nabla operator
∇^2	Laplacian operator

Subscripts

c	cold
h	hot
i	matrix index
j,k,p,q	matrix indices
∞	Reference state

Superscripts

i	elemental parameter
n	time step

Chapter 1

Introduction

1.1 A Review of the Numerical Methods

The techniques that are most commonly used to solve flow problems in computational fluid dynamics are the finite difference method, the finite element method, and the spectral method.

The finite difference method has been around the longest and is still popular because of its simplicity.

The finite difference method generally provides pointwise approximations to partial differential equations. Derivatives in the governing partial differential equations are replaced by equivalent finite difference expressions which involve the values of the solution at discrete grid points of the domain. Finite-difference method is easy to implement but it suffers from several disadvantages like low finite-order accuracy in evaluation of the derivatives, the difficulty in handling irregular geometries, the difficulty in imposing unusual boundary conditions along arbitrary boundaries, and the inability to employ nonuniform grids with ease.

Finite element method has been widely applied to many applications related to mechanical engineering, especially in solid mechanics, because of its extreme geometrical flexibility. These methods are also used to solve heat transfer and fluid flow problems.

Finite element methods provide piecewise, or regional approximation to partial differential equations. Various methods of this class exist; all requiring that an integral representation of a partial differential equation be constructed. Classical finite element methods for structural mechanics are based on variational principles. For

transient diffusion and conduction and for convective heat transfer processes more general approaches, such as a method of weighted residuals, are used. Finite element method is a low order h-type weighted residual method.

The principle advantage of the finite element approach for convective heat transfer is in the ability to handle irregular geometries. It generally requires fewer node points for a given accuracy as compared with finite difference methods. The drawback of the finite element method is that it is a low order method. Like finite difference methods, the finite element method converges slowly as the number of the elements is increased.

Finite difference and finite element methods are finite order accurate, i.e., the error of approximation behaves like $(1/N)^m$, where N is the number of nodal points and m the order of the scheme.

The spectral method is a high order weighted residual method [1].It is also known as the p-type weighted residual method.Unlike the finite element method, the trial functions of the spectral method are global, so it is usually applied to regular geometry problems with smooth solutions. The spectral method is known for achieving high accuracy. For equivalent number of grid points, spectral methods provide excellent accuracy compared with either finite-difference or finite-element methods. It has been estimated that in order to obtain 1% accuracy for a wave-like solution, 40 grid points per wavelength are needed for the second-order finite difference method,but only 3.5 collocation points per wavelength are needed for the Chebyshev spectral method. Therefore the spectral method is about 10 times more efficient than the finite difference method in storage aspect alone (in 1-D).Peyret and Taylor [10] compared the finite difference method with the spectral method and found that the spectral method was at least 10 times faster than the finite difference method for the same accuracy in the vortex problem they solved. Spectral methods display exponential convergence rates for increasing N. The convergence rate associated with the spectral methods depend only on the smoothness of the approximated function within the computational domain and the approximation error decreases faster than any finite power of 1/N, where N is the number of nodal points in the domain.

The basic idea of spectral method is to express the dependent variables in the form of a truncated expansion of orthogonal eigen-functions of the Sturm-Liouville problem. The coefficients of this expansion are determined using either a Galerkin or a Collocation formulation. The trial functions which are commonly used in spectral expansion include the Chebyshev, Legendre, and Laguerre polynomials for problems involving nonperiodic boundary conditions. For periodic problems the global inter-

polant is a Fourier series.

However, the spectral method has its own limitations. For instance, the grid interval is not uniform and it decreases drastically toward the boundaries of the computational domain. This imposes a severe limitation on the maximum time step when solving initial value problems via an explicit time marching scheme. Therefore, we often use implicit methods in conjuction with spectral algorithms. Unfortunately, these implicit schemes are not very efficient either, because the matrices in the spectral method are full matrices, unlike the narrow banded matrices of the finite difference and even the finite element methods. The main weakness of the spectral method relativite to FDM and FEM is its inflexibility to be adaptable to irregular computational domain. The solution of the physical problems should be smooth and the solution domain should be rectangular-like; otherwise spectral accuracy cannot be obtained. The appearance of 'spectral element method' that combines the generality of FEM and the accuracy of SM, has overcome the problem of restriction on the geometry.

1.2 Spectral-Element Method

The spectral element method (SEM) is a synthesis of the spectral and the finite element method [2,3]. The spectral element method is also called the 'p-type finite element' method, or the h-p type weighted residual method. Like the spectral method, it uses high order polynomials as trial functions,but like the finite element method, it decomposes the computational domain into many elements and defines local trial functions. The hybrid character of the spectral element method enables it to overcome the shortcomings of both the spectral method and the finite element method but still retain their advantages. Since the trial functions of the spectral element method are local, it can handle complex geometry easily. On the other hand, it is still a high order weighted residual method, so the exponential convergence rate is achieved as the degree of the polynomials in each element is increased. However, as with the conventional spectral method, the spectral accuracy can only be achieved when the solution possesses no singularities. In the spectral element approach, the spectral approximation is applied on each of the subdomains. Therefore, for those subdomains where the solutions are not smooth,the high order accuracy of spectral methods will be destroyed. The main difference between the spectral element method and the spectral multi-domain method is that the C^0 and C^1 boundary conditions at the interface of the elements have to be explicitly enforced by the spectral multi-domain method. The

spectral element method, by contrast, uses the variational principle to guarantee C^0 and C^1 (weakly) continuity at the interface,which results in a much simpler and more natural approach than the non-variational method; therefore, parallel algorithms can be conventiently implemented [3].

Chapter 2

Mathematical Formulation

2.1 Introduction

The spectral element method can be applied to simple (e.g., rectangular, square domains) as well as arbitrary (curved) geometries. However, for complicated geometries the technique can be applied only after coordinate transformation. The complicated geometry is first changed into a simple geometry (rectangular or square) by some isoparametric transformation and the technique is then applied. Any complex geometry in two dimensional space can be broken into multiple elements of standard rectangular or quadrilateral shapes.

In the spectral element discretization, the computational domain is broken into a number of elements, and within each element the dependent variable is represented as a high-order Lagrangian interpolant, in terms of Chebyshev polynomials, the coefficients of which are related to the function values at the Gauss-Lobatto Chebyshev collocation points.

The governing equations are partially discretized using finite difference approximation for the time derivative. The convective and source terms are treated explicitly and the diffusion term (elliptic contribution) implicitly.

Table 2.1: Expressions for ϕ, Γ_ϕ and S_ϕ in general transport equation (dimensional form)

Equation	ϕ	Γ	S_ϕ
Continuity	1	0	0
x momentum	u	μ	$-\frac{\partial p}{\partial x} + (\rho_\infty - \rho)g_x$
y momentum	v	μ	$-\frac{\partial p}{\partial y} + (\rho_\infty - \rho)g_y$
Energy	T	$\frac{k}{c_p}$	$\frac{1}{c_p}[\mu\Phi + q'''']$

Table 2.2: Expressions for ϕ, Γ_ϕ and S_ϕ in general transport equation (nondimensional form)

Equation	ϕ	Γ	S_ϕ
Continuity	1	0	0
x momentum	u	$\frac{1}{R_e^2}$	$-\frac{\partial p}{\partial x} + S_u$
y momentum	v	$\frac{1}{R_e^2}$	$-\frac{\partial p}{\partial y} + S_v$
Energy	θ	$\frac{1}{P_r}$	S_T

2.2 Governing Equations for Laminar Incompressible Flow

The general transport equation for the flow property ϕ in cartesian coordinates can be written as

$$\rho\frac{\partial\phi}{\partial\tau} + \rho(U\frac{\partial\phi}{\partial X} + V\frac{\partial\phi}{\partial Y}) = \Gamma\left[\frac{\partial^2\phi}{\partial X^2} + \frac{\partial^2\phi}{\partial Y^2}\right] + S_\phi \tag{2.1}$$

Where S_ϕ is a source term , Γ is a diffusion coefficient. The parameter ϕ represents 1, u , v , T , ω, ψ , or θ . A summary of the S_ϕ and Γ_ϕ applicable to each ϕ is given in Table 2.1.

Writing the general transport equation in a dimensionless form facilitates generalisation to embody a class of problems. In the usual dimensionless form of the general transport equation the parameters are defined in a way as given in Table 2.2.

Table 2.3: Expressions for ϕ, ρ, Γ_ϕ and S_ϕ : $(\psi - \omega)approach$

Function	ϕ	ρ	Γ	S_ϕ
Temperature	θ	1	$\frac{1}{P_r}$	S_T
Vorticity	ω	1	1	S_ω
Stream function	ψ	0	1	ω

If the governing dimensionless equations for the conservation of mass , momentum and energy are formulated in terms of vorticity ,stream function and temperature then the parameters used in general transport equation (2.1) are defined in Table 2.3.

2.3 Time Discretization

Finite-difference approximaton is used to handle time dependent term. Both explicit and implicit methods have been used to a variety of flow situations. Generally, the implicit methods have been recommended because of their favourable stability properties. The explicit schemes for parabolic unsteady partial differential equations are required to satisfy certain stability requirements, which impose a restriction on the time step. Since the implicit methods are generally free from these restrictions, it may be possible to use a relatively larger time step than what is permissible in explicit schemes. However, an implicit method has its own limitations. An implicit scheme requires a relatively large number of arithmatic operations than an explicit scheme. For a coupled non-linear partial differential equation set, the implicit formulation will be even more time consuming because an iterative scheme is required to take care of the non-liearities and the coupling in the governing equations.

Patera [2,3] uses an Adams-Bashforth Crank-Nicolson (ABCN) scheme with a spectral element spatial discretization.

To solve the general transport equation [Eqn (2.1)], a semi-implicit, time-marching scheme is employed for time discretization, wherein all the linear terms (continuity, pressure and diffusion terms) are treated implicitly and the non-linear convective terms explicitly. The time-discretized form of equation (2.1) is given by

$$\frac{\phi^{n+1} - \phi^n}{\Delta\tau} + \left[U\frac{\partial\phi}{\partial X} + V\frac{\partial\phi}{\partial Y}\right]^n = \frac{\Gamma}{\rho}\left[\frac{\partial^2\phi}{\partial X^2} + \frac{\partial^2\phi}{\partial Y^2}\right]^{n+1} + \frac{S_\phi^n}{\rho} \tag{2.2}$$

which can be rearranged in the form

$$\left(\frac{\partial^2\phi}{\partial X^2}\right)^{n+1} + \left(\frac{\partial^2\phi}{\partial Y^2}\right)^{n+1} - \frac{\phi^{n+1}}{\Gamma\Delta\tau/\rho} = -\frac{\phi^n}{\Gamma\Delta\tau/\rho} + \frac{1}{\Gamma/\rho}\left[U\frac{\partial\phi}{\partial X} + V\frac{\partial\phi}{\partial Y}\right]^n - \frac{S_\phi^n}{\Gamma} \quad (2.3)$$

or

$$\phi_{xx} + \phi_{yy} - \lambda^2\phi = f \quad (2.4)$$

This is the well known Helmholtz (Second-order elliptic) equation. The function ϕ is unknown function to be computed and ' f ' is the known forcing function. Here n refer to the known values at time τ, while all other values, $n+1$, are unknown values at time $\tau + \Delta\tau$. The parameter λ^2 can take different positive values. In the limiting case when $\lambda^2 \longrightarrow 0$, equaton (2.4) reduces to Poisson equation, which too can be solved using the Helmholtz solver.

2.4 Spectral Element Spatial Discretization

In order to solve the Helmholtz equation [Eqn. (2.4)] by spectral element method we use its equavalent variational formulation (as in the finite-element technique) which amounts to the maximization of the functional

$$I = \int\int \left[-\frac{1}{2}\{(\phi_x)^2 + (\phi_y)^2\} - \frac{\lambda^2}{2}\phi^2 - \phi f\right] dxdy \quad (2.5)$$

The integration in equation (2.5) spans over the entire computational domain.

When the domain is broken up into M elements, the functional will simply be the summation of the contributions from the individual elements, namely

$$I = \sum_{i=1}^{M} I^i \quad (2.6)$$

For the i^{th} element the functional, I^i, is given by

$$I^i = \int\int \left[-\frac{1}{2}\{(\phi_x{}^i)^2 + (\phi_y{}^i)^2\} - \frac{\lambda^2}{2}(\phi^i)^2 - \phi^i f^i\right] dxdy \quad (2.7)$$

The intregration in equation (2.7) spans over the area of the i^{th} element , defined as the rectangle between $[a_x^i, b_x^i]$ and $[a_y^i, b_y^i]$. (In this study we use only rectangular elements.).

Within the i^{th} element the variable $\phi(x,y)$ is represented as a Lagrangian interpolant, in terms of Chebyshev polynomials, through $(N_x^i+1)(N_y^i+1)$ Gauss-Lobatto Chebyshev points given by

$$\bar{x}_j^i = cos(\frac{\pi j}{N_x^i}) \qquad j = 0,1,2,...,N_x^i \tag{2.8}$$

$$\bar{y}_k^i = cos(\frac{\pi k}{N_y^i}) \qquad k = 0,1,2,...,N_y^i \tag{2.9}$$

The Lagrangian interpolant of a variable $\phi(x,y)$ in the i^{th} element (of dimensions $L_x^i \times L_y^i$) is given by

$$\phi^i(\bar{x}^i,\bar{y}^i) = \sum_{j=0}^{N_x^i}\sum_{k=0}^{N_y^i} \phi_{jk}^i h_j^i(\bar{x}^i) h_k^i(\bar{y}^i) \tag{2.10}$$

where ϕ_{jk}^i are the values of ϕ at the point $(\bar{x}_j,\bar{y}_k)$ and $(\bar{x},\bar{y})$ is the local coordinate system normalised so that the rectangular elements lie between $\bar{x} = \pm 1, \bar{y} = \pm 1$.

The local i^{th} element coordinate system is therefore defined as

$$\bar{x}^i = \frac{2}{L_x^i}(x - a_x^i) - 1 \tag{2.11}$$

$$\bar{y}^i = \frac{2}{L_y^i}(y - a_y^i) - 1 \tag{2.12}$$

where $L_x^i(= b_x^i - a_x^i)$ and $L_y^i(= b_y^i - a_y^i)$ are the lengths of the element in the x and y directions respectively.

A local coordinate system (i.e., a coordinate system in the element) proves to be convenient in the use of the interpolation functions.The global coordinate x (which is used to describe the governing differential equations of the problem) can be retrieved from the local coordinate by inverting the linear transformation given by equations (2.11) and (2.12).

The x direction interpolation functions $h_m(\bar{x})$ are N_x^{ith} order local Lagrangian interpolants in terms of Chebyshev polynomials satisfying

$$h_m^i(\bar{x}_n^i) = \delta_{mn} \tag{2.13}$$

within the element (at the local coordinates); δ_{mn} is the Kronecker-delta symbol and $\bar{x}_n$ denotes the x coordinate of the n^{th} Gauss-Lobatto point in the x direction. h_m^i are identically zero outside the i^{th} element.

The interpolation functions $h_m^i(\bar{x}^i)$can then be expressed as

$$h_j^i(\bar{x}^i) = \frac{2}{N_x^i} \sum_{n=0}^{N_x^i} \frac{1}{\bar{C}_j \bar{C}_n} T_n(\bar{x}_j^i) T_n(\bar{x}^i) \tag{2.14}$$

where the T_n are the n^{th} order Chebyshev polynomials.The Chebyshev polynomials $T_n(\bar{x})$ are

$$T_n(cos\theta) = cos(n\theta) \tag{2.15}$$

or

$$T_n(\bar{x}) = cos(ncos^{-1}\bar{x}) \tag{2.16}$$

and therefore

$$T_n(\bar{x}_j) = cos(\frac{\pi n j}{N_x^i}) \tag{2.17}$$

also in equation (2.14), the integer functions $\bar{C}$ are

$$\bar{C}_k = 1, \qquad for \quad k \neq 0 \quad or \quad N_x^i \tag{2.18}$$

$$= 2, \qquad for \quad k = 0 \quad or \quad N_x^i \tag{2.19}$$

We approximate the variable ϕ in the i^{th} element by

$$\phi \approx \phi_N = \sum_{j=0}^{N_x} \sum_{k=0}^{N_y} \phi_{jk} h_j(\bar{x}) h_k(\bar{y}) \tag{2.20}$$

where $h_k(\bar{y})$ are interpolation functions similar to $h_m(\bar{x})$ explained above, except that it is for N_y^i points.

We can compute the maximum error in the domain between the exact solution and the calculated solution ϕ_N using the norm

$$\| \phi - \phi_N \| = max|\phi(\bar{x}, \bar{y}) - \phi_N(\bar{x}, \bar{y})| \tag{2.21}$$

for

$$-1 \leq \bar{x} \leq 1 \qquad\qquad -1 \leq \bar{y} \leq 1$$

This measure of difference is called supmetric.Note that the supmetric is a real number indicative of error. This error reduces very fast as the number of points is increased in a spectral method.

With these particular collocation points, the Lagrangian interpolant for ϕ^i satisfies

$$\| \phi - \phi^i \| \ll (\frac{1}{N_x^i N_y^i})^k, \qquad N_x^i N_y^i \longrightarrow \infty \tag{2.22}$$

for all finite k. This property is called 'exponential' or 'infinite-order' accuracy of interpolation.

Other choices of collocation points have the property (2.22), however, (2.8) and (2.9) seems a reasonable choice given the good approximation properties of Chebyshev polynomials as well as the existence of a fast transform for Chebyshev series.

2.5 Formation of Elemental Equations

The forcing function f, in Helmholtz equation (2.4) is also interpolated in the same fashion as ϕ is interpolated.For i^{th} element

$$f^i(\bar{x}^i, \bar{y}^i) = \sum_{j=0}^{N_x^i} \sum_{k=0}^{N_y^i} f_{jk}^i h_j^i(\bar{x}^i) h_k^i(\bar{y}^i) \tag{2.23}$$

noting that

$$h_j^i(\bar{x}^i) = \frac{2}{N_x^i} \sum_{n=0}^{N_x^i} \frac{1}{\bar{C}_j \bar{C}_n} T_n(\bar{x}_j^i) T_n(\bar{x}^i) \tag{2.24}$$

$$h_k^i(\bar{y}^i) = \frac{2}{N_y^i} \sum_{m=0}^{N_y^i} \frac{1}{\bar{C}_k \bar{C}_m} T_m(\bar{y}_k^i) T_m(\bar{y}^i) \tag{2.25}$$

Therefore

$$\phi^i(\bar{x}^i, \bar{y}^i) = \frac{4}{N_x^i N_y^i} \sum_{j=0}^{N_x^i} \sum_{k=0}^{N_y^i} \sum_{n=0}^{N_x^i} \sum_{m=0}^{N_y^i} \phi_{jk}^i \frac{1}{\bar{C}_j \bar{C}_n \bar{C}_k \bar{C}_m} T_n(\bar{x}_j^i) T_n(\bar{x}^i) T_m(\bar{y}_k^i) T_m(\bar{y}^i) \tag{2.26}$$

and

$$f^i(\bar{x}^i, \bar{y}^i) = \frac{4}{N_x^i N_y^i} \sum_{j=0}^{N_x^i} \sum_{k=0}^{N_y^i} \sum_{n=0}^{N_x^i} \sum_{m=0}^{N_y^i} f_{jk}^i \frac{1}{\bar{C}_j \bar{C}_n \bar{C}_k \bar{C}_m} T_n(\bar{x}_j^i) T_n(\bar{x}^i) T_m(\bar{y}_k^i) T_m(\bar{y}^i) \tag{2.27}$$

In order to apply spectral element method involving Chebyshev polynomials each element should be mapped (using linear transformation equations (2.11) and (2.12)) onto a domain spanning from -1 to +1 in $\bar{x}$ and $\bar{y}$ directions respectively, because Chebyshev polynomials itself are defined over this span. Whenever a differentiation or integration is performed in the transformed co-ordinate $(\bar{x}, \bar{y})$, it should be properly scaled.

Since

$$\bar{x} = \frac{2}{L_x}(x - a_x) - 1 \tag{2.28}$$

We have

$$d\bar{x} = \frac{2}{L_x}dx \tag{2.29}$$

The differentials with respect to x , ϕ_x and $\phi_{\bar{x}}$ in the two coordinate systems are related by

$$\frac{\partial \phi}{\partial x} = \frac{\partial \phi}{\partial \bar{x}}\frac{\partial \bar{x}}{\partial x} = \frac{2}{L_x}\frac{\partial \phi}{\partial \bar{x}} \tag{2.30}$$

$$\frac{\partial \phi}{\partial y} = \frac{\partial \phi}{\partial \bar{y}}\frac{\partial \bar{y}}{\partial y} = \frac{2}{L_y}\frac{\partial \phi}{\partial \bar{y}} \tag{2.31}$$

where $\frac{2}{L_x}$ and $\frac{2}{L_y}$ are scale factors. The derivatives $\frac{\partial \phi}{\partial \bar{x}}$ and $\frac{\partial \phi}{\partial \bar{y}}$ can be obtained as

$$\frac{\partial \phi^i}{\partial \bar{x}^i} = \sum_{j=0}^{N_x^i}\sum_{k=0}^{N_y^i} \phi_{jk}^i \frac{dh^i(\bar{x}^i)}{d(\bar{x}^i)} h_k^i(\bar{y}^i) \tag{2.32}$$

After substitution this equation reduces to

$$\frac{\partial \phi^i}{\partial \bar{x}^i} = \sum_{j=0}^{N_x^i}\sum_{k=0}^{N_y^i} \phi_{jk}^i \frac{2}{N_x^i}\sum_{n=0}^{N_x^i}\frac{1}{\bar{C}_j\bar{C}_n}T_n(\bar{x}_j^i)\frac{dT_n(\bar{x}^i)}{d(\bar{x}^i)}\frac{2}{N_y^i}\sum_{m=0}^{N_y^i}\frac{1}{\bar{C}_k\bar{C}_m} T_m(\bar{y}_k^i)T_m(\bar{y})^i \tag{2.33}$$

The resulting expression may be written as

$$(\frac{\partial \phi}{\partial x})^i = \frac{2}{L_x^i}\frac{4}{N_x^i N_y^i}\sum_{j=0}^{N_x^i}\sum_{k=0}^{N_y^i}\sum_{n=0}^{N_x^i}\sum_{m=0}^{N_y^i} \phi_{jk}^i \frac{1}{\bar{C}_j\bar{C}_n\bar{C}_k\bar{C}_m}T_n(\bar{x}_j^i)T_m(\bar{y}_k^i) \frac{dT_n(\bar{x}^i)}{d(\bar{x}^i)}T_m(\bar{y}^i) \tag{2.34}$$

Similarly

$$(\frac{\partial \phi}{\partial y})^i = \frac{2}{L_y^i}\frac{4}{N_x^i N_y^i}\sum_{j=0}^{N_x^i}\sum_{k=0}^{N_y^i}\sum_{n=0}^{N_x^i}\sum_{m=0}^{N_y^i}\phi_{jk}^i \frac{1}{\bar{C}_j\bar{C}_n\bar{C}_k\bar{C}_m} T_n(\bar{x}_j^i)T_m(\bar{y}_k^i) \\ T_n(\bar{x}^i)\frac{dT_m(\bar{y}^i)}{d(\bar{y}^i)} \tag{2.35}$$

We now insert the interpolants (2.26), (2.27), (2.34), and (2.35) into the functional (2.7), perform the resulting integrals, and require stationarity with respect to variations in the ϕ_{jk}^i, i.e., require that the variation of I^i with respect to the nodal values ϕ_{jk}^i vanish :

$$\frac{\delta I^i}{\delta \phi_{jk}^i} = 0 \tag{2.36}$$

Remember that

$$\frac{\partial}{\partial \phi_{jk}^i}(\phi_{pq}^i) = \delta_{pj}\delta_{qk} \tag{2.37}$$

Then the elemental algebraic system of equations will simply be

$$C_{jklm}^i \phi_{lm}^i = B_{jklm}^i f_{lm}^i = e_{lm}^i \tag{2.38}$$

$$C_{jklm}^i = A_{jklm}^i - \lambda^2 B_{jklm}^i \tag{2.39}$$

Here

$$A_{jklm}^i = -\frac{L_y^i}{L_x^i}\frac{1}{(N_x^i N_y^i)^2}\tilde{A}_{jl}^{i,x}\tilde{B}_{km}^{i,y} - \frac{L_x^i}{L_y^i}\frac{1}{(N_x^i N_y^i)^2}\tilde{A}_{km}^{i,y}\tilde{B}_{jl}^{i,x} \tag{2.40}$$

$$B_{jklm}^i = \frac{L_x^i L_y^i}{4}\frac{1}{(N_x^i N_y^i)^2}\tilde{B}_{jl}^{i,x}\tilde{B}_{km}^{i,y} \tag{2.41}$$

$$\tilde{A}_{jl}^{i,x} = \frac{4}{\bar{C}_j\bar{C}_l}\sum_{n=0}^{N_x^i}\sum_{m=0}^{N_y^i}\frac{1}{\bar{C}_n\bar{C}_m}T_n(\bar{x}_j^i)T_m(\bar{x}_l^i)a_{nm} \tag{2.42}$$

$$\tilde{B}_{jl}^{i,x} = \frac{4}{\bar{C}_j\bar{C}_l}\sum_{n=0}^{N_x^i}\sum_{m=0}^{N_y^i}\frac{1}{\bar{C}_n\bar{C}_m}T_n(\bar{x}_j^i)T_m(\bar{x}_l^i)b_{nm} \tag{2.43}$$

and

$$\begin{aligned} a_{nm} &= \int_{-1}^{1} \frac{dT_n}{d\bar{x}^i}\frac{dT_m}{d\bar{x}^i}d\bar{x}^i \\ &= 0, \qquad n+m \quad odd \\ &= \frac{nm}{2}[J_{|(n-m)/2|} - J_{|(n+m)/2|}], \qquad n+m \quad even \end{aligned} \tag{2.44}$$

Where

$$\begin{aligned} J_k &= -4\sum_{p=1}^{k}\frac{1}{2p-1}, \qquad k \geq 1 \\ &= 0, \qquad k = 0 \end{aligned} \tag{2.45}$$

Also

$$\begin{aligned} b_{nm} &= \int_{-1}^{1} T_n T_m d\bar{x}^i \\ &= 0, \qquad n+m \quad odd \\ &= \frac{1}{1-(n+m)^2} + \frac{1}{1-(n-m)^2}, \qquad n+m \quad even \end{aligned} \tag{2.46}$$

2.6 Formation of Global Matrix Equations

Once the system of discrete equations for each element is obtained, with proper boundary conditions imposed for the elements having one or more sides lying on the boundary of the computational domain, the system of global matrices is then constructed by 'direct stiffness' summation, adding at the boundary nodes the contributions from the corresponding elements.

Owing to the difficulty in direct implementation with four dimensional arrays [B] and [C] in equation (2.38), this elemental matrix equation is transformed into a more conventional form by combining the two indices j and k to give a third index p, and the indices l and m to give a third index q by the following equations

$$p = (N_y + 1).j + k \tag{2.47}$$

where

$$j = 0, 1, ..., N_x, \qquad k = 0, 1, ..., N_y$$

so

$$p = 0, 1, ..., (N_x + 1).(N_y + 1) - 1 \tag{2.48}$$

and

$$q = (N_y + 1).l + m \tag{2.49}$$

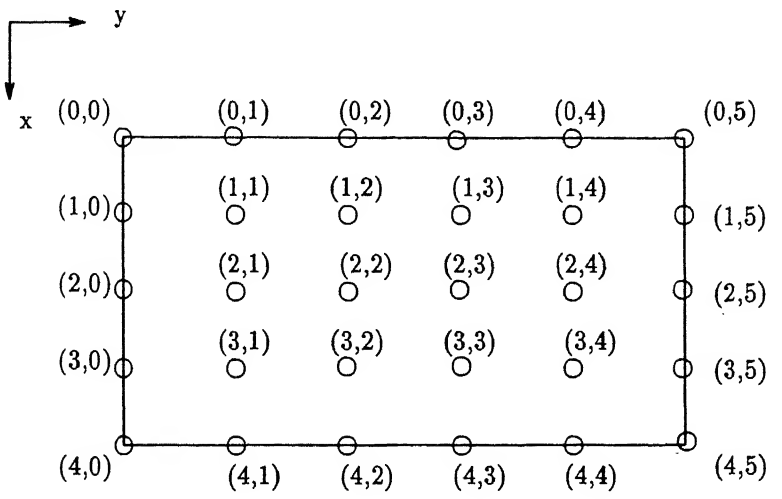

Figure 2.1: Original numbering of grid points in an element

$$l = 0, 1, ..., N_x, \qquad m = 0, 1, ..., N_y$$

or

$$q = 0, 1, ..., (N_x + 1).(N_y + 1) - 1 \tag{2.50}$$

when this is done, equation (2.38) is transformed to convetional matrix form

$$C^i_{pq}\phi^i_q = B^i_{pq}f^i_q = e^i_p \tag{2.51}$$

Any grid point in an element, which was specified by two indices in equation (2.38), is now specified by a single index, say p following the above transformation. This changed numbering system for $N_x = 4$ and $N_y = 5$ is illustrated in Figure 2.1. The x direction is taken to be vertically downward and y direction horizontally rightward.

Based on the problem requirements, the computational domain may consist of a number of elements. The following remarks can be made on the comparison of the multi-elements and single-element case, keeping the total number of grid points in the computational domain exactly the same in both the cases [11].

- The single-element method will give a higher order approximation.
- The multi-element method will give greater geometric flexibility.
- The global matrix for the single-element case will be full while that of the multi-elements case will be relatively sparse. If this sparsity can be exploited by the solution procedure the multi-element method can be made more efficient in terms of computer time and memory.

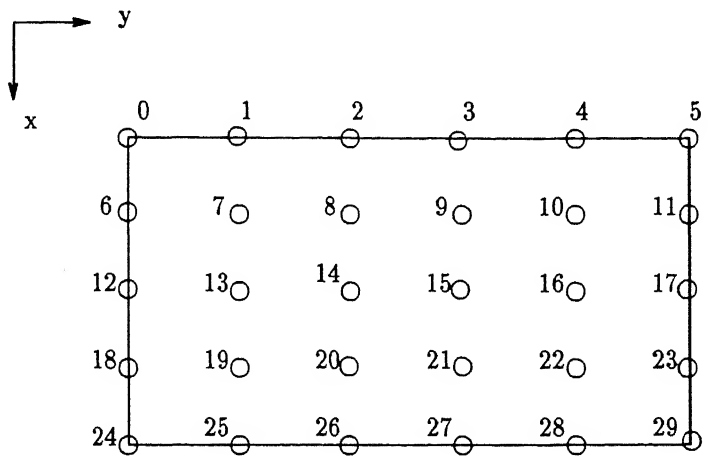

Figure 2.2: Changed numbering of grid points in an element

The higher order approximation in single element case results in higher accuracy compared to multiple elements. The accuracy depends upon the order of the Lagrangian interpolants and not on the total number of grid points. In multi-element case, to keep the total number of grid points same in the domain, the number of points per element get reduced and consequently the function will be approximated by a lower order interpolant, thereby causing deteriotion in the solution.

The conclusion drawn from the above discussion is that the main advantage of using multiple elements over single element lies in the greater geometric flexibility afforded by the former.

The total number of grid points in the domain in case of single element will be $(N_x + 1)(N_y + 1)$. The corresponding coefficient matrix [C] will be of order $(N_x + 1)(N_y + 1) \times (N_x + 1)(N_y + 1)$. If a rectangular domain consists of e_x elements in the x direction and e_y elements in the y direction, then the total number of grid points in the domain for $e_x \times e_y$ elements will be $(N_x.e_x+1)(N_y.e_y+1)$ and the global coefficient matrix $[C^{global}]$ will be of the order $(N_x.e_x + 1)(N_y.e_y + 1) \times (N_x.e_x + 1)(N_y.e_y + 1)$.

The global grid points numbering for a system of 2 elements in x direction and 2 elements in y direction, i.e., $e_x = 2$ and $e_y = 2$ and $N_x = 4, N_y = 5$ is shown in Figure 2.3. Listed in parenthesis are the element numbers, e.g., (k,l) represents the $(k, l)^{th}$ element in the domain.

The global numbering of grid points of $(k, l)^{th}$ element is as follows:

- gird point numbering on left face of $(k, l)^{th}$ element is given by
  $(N_y.e_x + 1)\{(k-1)N_x + i\} + (N_y.l + 1) - N_y$

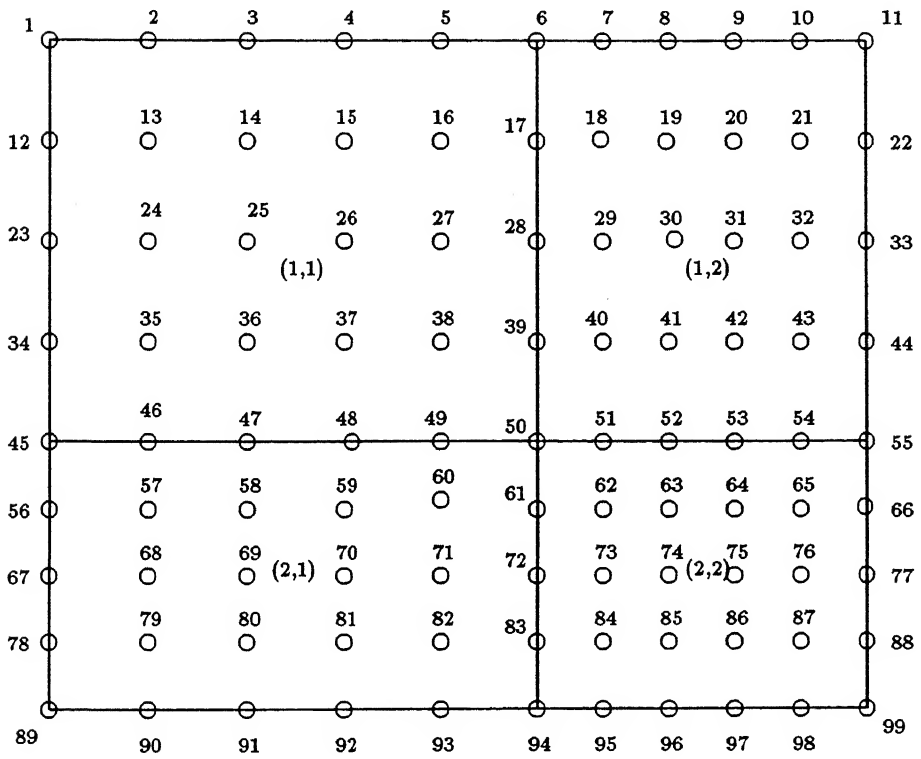

Figure 2.3: Global numbering of grid points in the computational domain

- grid point numbering on right face of $(k,l)^{th}$ element is given by $(N_y.e_x+1)\{(k-1)N_x+i\}+(N_y.l+1)$

Every grid point in the computational domain has two numbers associated with it: a local and a global number, as shown in Figures 2.2 and 2.3. The local number corresponds to its position in its element and the global number corresponds to its position in the whole computational domain.

Construction of global matrix, $[C^{global}]$, from elemental matrices, $[C]$, can be accomplished as follows:

For every point that lies in the interior of an element, the coefficients of the elemental matrix [C] in a locally numbered row and column are transferred to the corresponding globally numbered row and column in the global matrix $[C^{global}]$ without any modification in nodal values. Same procedure is applied for elemental matrix { e } and global matrix $\{e^{global}\}$. In doing so, a proper correspondence is made between the local and global number of the grid point in the domain.

However, at the intersection of the elemental boundaries in the domain, the equations corresponding to grid points at the interface of the two elements are obtained by adding the two equations corresponding to these grid points in the two elemental sets.

The global equations then are

$$C^{global}_{p_g q_g}\phi^{global}_{q_g} = e^{global}_{p_g} \tag{2.52}$$

where the ϕ^{global} vector incorporates all the unknown ϕ_{lm} of all the elements and the indices p_g and q_g represent the global indices, given by

$$\begin{aligned} p_g &= 1,...,(N_x.e_x+1).(N_y.e_y+1) \\ q_g &= 1,...,(N_x.e_x+1).(N_y.e_y+1) \end{aligned} \tag{2.53}$$

The inversion of the global system matrix is carried out directly (LU decomposition) in a preprocessing stage at the beginning of the simulation. Thereafter,only matrix multiplications are performed at each time step,which is very convenient regarding processing time.

2.7 Imposition of Boundary Conditions

2.7.1 Imposition of Dirichlet Boundary Conditions

Dirichlet boundary conditions are imposed by matrix condensation. The rows and columns corresponding to boundary points are eliminated from the system matrix.

There is another way of imposing these boundary conditions. The diagonal elements of $[C^{global}]$ in equation(2.52) corresponding to the boundary points are equated to a very large number and the corresponding elements in the right side of $\{e^{elobal}\}$ are set equal to the specified boundary value multiplied by the same large number. Then the resulting matrix equation is solved to obtain the same solution. This method is more expensive as it solves the full matrix equation with all points rather than just the points where the values are unknown. However, it has the advantage of simplicity of implementation.

2.7.2 Imposition of Neumann Boundary Conditions

Mathematical treatment of the spectral element technique is such that the zero Neumann conditions are naturally imposed and no modification of the matrix equations (2.38) is needed to impose these boundary conditions. However, non-zero Neumann conditions are imposed by modifying the functional (2.5).

To illustrate the procedure to impose the non-zero Neumann conditions, let us assume that

$$\frac{\partial \phi}{\partial x} = A(y) \qquad at \quad x = a_x^i \tag{2.54}$$

and the boundary of this element coincides with the boundary of the domain.

According to variational formulation, solution of the differential equation [Eq.(2.4)] subject to given boundary condition [Eq.(2.54)] is equivalent to maximization of the functional

$$I(\phi) = \int\int \left[-\frac{1}{2}\{(\phi_x)^2 + (\phi_y)^2\} - \frac{\lambda^2}{2}\phi^2 - \phi f \right] dxdy + I_{bc} \tag{2.55}$$

where I_{bc} is the boundary term corresponding to the non-zero Neumann condition [Eq.(2.54)]. For each element i which has that boundary condition in the domain, Eq.(2.7) can be written as

$$I^i(\phi) = \int_{a_x^i}^{b_x^i} \int_{a_y^i}^{b_y^i} \left[-\frac{1}{2}\{(\phi_x{}^i)^2 + (\phi_y{}^i)^2\} - \frac{\lambda^2}{2}(\phi^i)^2 - \phi^i f^i \right] dxdy + \tag{2.56}$$

$$\int_{a_x^i}^{b_x^i}\int_{a_y^i}^{b_y^i}\{-A(y)\phi\}dy|_{x=a_x^i}$$

i.e.,

$$I^i = I^i_{interior} + I^i_{a_x} \tag{2.57}$$

Because of the additional term in equation (2.57) compared to equation (2.5), the final elemental matrix equation [Eq.(2.38)] corresponding to the grid points on this boundary will have some additional terms in the right hand side. These terms can be determined as follows:

The interpolant of variable ϕ on this boundary of i^{th} element is a function of y only, i.e.,

$$\phi|_{x=a_x^i} = \sum_{k=0}^{N_y{}^i}\phi^i_{Nxk}\frac{2}{N_y^i}\sum_{n=0}^{N_y^i}\frac{1}{\bar{C}_k\bar{C}_n}T_n(\bar{y}^i_k)T_n(\bar{y}^i) \tag{2.58}$$

similarly

$$A(y) = \sum_{j=0}^{N_y{}^i}A_j\frac{2}{N_y^i}\sum_{m=0}^{N_y^i}\frac{1}{\bar{C}_j\bar{C}_m}T_m(\bar{y}^i_j)T_m(\bar{y}^i) \tag{2.59}$$

Therefore

$$\begin{aligned} I^i_{a_x} &= -\int_{a_y^i}^{b_y^i}\{A\phi^i\}|_{x=a_x^i}dy \qquad (2.60)\\ &= -\int_{-1}^{1}A(\bar{y}).\phi(\bar{y}).\frac{L_y^i}{2}d\bar{y}\\ &= -\frac{L_y^i}{2}\int_{-1}^{1}\sum_{j=0}^{N_y{}^i}A_j\frac{2}{N_y^i}\sum_{m=0}^{N_y^i}\frac{1}{\bar{C}_j\bar{C}_m}T_n(\bar{y}^i_j)T_n(\bar{y}^i)\sum_{k=0}^{N_y{}^i}\phi^i_{Nxk}\frac{2}{N_y^i} \end{aligned}$$

$$\sum_{n=0}^{N_y^i}\frac{1}{\bar{C}_k\bar{C}_n}T_n(\bar{y}^i_k)T_n(\bar{y}^i)$$

$$= -\frac{2L_y^i}{N_y^{i2}}\sum_{j=0}^{N_x^i}\sum_{k=0}^{N_y^i}\sum_{n=0}^{N_x^i}\sum_{m=0}^{N_y^i}A_j\phi^i_{Nxk}\frac{1}{\bar{C}_j\bar{C}_n\bar{C}_k\bar{C}_m}T_m(\bar{y}^i_j)T_n(\bar{y}^i_k)$$

$$\int_{-1}^{1}T_m(\bar{y}^i)T_n(\bar{y}^i)d\bar{y}$$

hence

$$I^i_{a_x} = -\frac{2L_y^i}{N_y^{i2}}\sum_{j=0}^{N_x^i}\sum_{k=0}^{N_y^i}\sum_{n=0}^{N_x^i}\sum_{m=0}^{N_y^i}A_j\phi^i_{Nxk}\frac{T_m(\bar{y}^i_j)T_n(\bar{y}^i_k)}{\bar{C}_j\bar{C}_n\bar{C}_k\bar{C}_m}b_{nm} \tag{2.61}$$

where the integration term b_{nm} is defined in equation (2.46).

In order to maximize I^i, we require that the variations of this with respect to the nodal values ϕ^i_j on $x = a^i_x$ boundary vanish. In this maximization, $I^i_{a_x}$ contributes only to those nodal equations which are obtained by differentiating I^i w.r.t. nodal values ϕ^i_{Nxk} which lie on the boundary $x = a^i_x$. The contribution of $I^i_{a_x}$ is

$$-\frac{2}{L^i_y}\sum_{j=0}^{N^i_y}\sum_{n=0}^{N^i_x}\sum_{m=0}^{N^i_y} A_k \frac{T_n(\bar{y}^i_k)T_m(\bar{y}^i_j)}{\bar{C}_j\bar{C}_n\bar{C}_k\bar{C}_m} b_{nm} \tag{2.62}$$

which is added to the right hand side of equation (2.38) for node ϕ^i_{Nxk}.

Similar treatment can be done for other boundaries.

2.8 Spatial Derivatives at Collocation points

Spectral element method allows extremely accurate evaluation of derivatives in each element in the computational domain.

The spatial derivatives of the variable ϕ with respect to x and y are given by equations (2.35) and (2.36). In i^{th} element, equation (2.36) can be rewritten as

$$\frac{\partial\phi}{\partial x} = \frac{2}{L_x}\frac{2}{N_x}\sum_{j=0}^{N_x}\sum_{k=0}^{N_y}\sum_{n=0}^{N_x} \phi_{jk}\frac{1}{\bar{C}_j\bar{C}_n}T_n(\bar{x}_j)\frac{dT_n(\bar{x})}{d\bar{x}}h_k(\bar{y}) \tag{2.63}$$

Using the definition of Gauss-Lobatto Chebyshev points and that of Chebyshev polynomials, we have

$$T_n(\bar{x}_j) = cos\left[n.cos^{-1}(cos\frac{\pi j}{N_x})\right] = cos\frac{n\pi j}{N_x} \tag{2.64}$$

and

$$\frac{dT_n(\bar{x})}{d\bar{x}} = \frac{n.sin\left[n.cos^{-1}(\bar{x}\right]}{\sqrt{(1-\bar{x}^2)}} \tag{2.65}$$

substitution of (2.64) and (2.65) in (2.63) yields

$$\frac{\partial\phi}{\partial x} = \frac{2}{L_x}\frac{2}{N_x}\sum_{j=0}^{N_x}\sum_{k=0}^{N_y}\sum_{n=0}^{N_x} \phi_{jk}\frac{1}{\bar{C}_j\bar{C}_n}cos(\frac{n\pi j}{N_x})\frac{n.sin\left[n.cos^{-1}(\bar{x}\right]}{\sqrt{(1-\bar{x}^2)}}h_k(\bar{y}) \tag{2.66}$$

As the function is represented by its values at the collocation points, its derivative will also be given by at these collocation points. For any point $x = x_r$, we obtain, from equation (2.66)

$$\frac{\partial\phi}{\partial x_r} = \frac{2}{L_x}\frac{2}{N_x}\sum_{j=0}^{N_x}\sum_{k=0}^{N_y}\sum_{n=0}^{N_x} \phi_{jk}\frac{1}{\bar{C}_j\bar{C}_n}cos(\frac{n\pi j}{N_x})\frac{n.sin\frac{n\pi r}{N_x}}{sin\frac{\pi r}{N_x}}h_k(\bar{y}) \tag{2.67}$$

For fixed $\bar{y} = \bar{y}_p$, the term $h_k(\bar{y})$ in equation (2.67) is $= \delta_{kp}$ and the summation over k can be dropped upon substituting ϕ_{jp} for ϕ_{jk}. The resulting expression takes the form

$$\frac{\partial \phi}{\partial x_r} = \frac{2}{L_x}\frac{2}{N_x}\sum_{j=0}^{N_x}\sum_{n=0}^{N_x}\phi_{jp}F_{nj}DP_{nr} \tag{2.68}$$

where

$$F_{nj} = \frac{1}{\bar{C}_j\bar{C}_n}cos\frac{n\pi j}{N_x} \tag{2.69}$$

and

$$\begin{aligned} DP_{nr} &= \frac{n.sin\frac{n\pi r}{N_x}}{sin\frac{\pi r}{N_x}} \qquad r \neq 0 \quad or \quad N_x \\ &= n^2 \qquad\qquad r = 0 \\ &= (-1)^{n-1}n^2 \qquad\qquad r = N_x \end{aligned} \tag{2.70}$$

Similar treatment works to evaluate derivative with respect to y.

Chapter 3

Test Problems

3.1 Unsteady Natural Convection in a Rectangular Cavity

The study of natural convection in enclosures is of considerable interest because of its importance in numerous engineering applications such as the cooling of electronic equipments, materials processing, solar energy systems, thermal energy storage systems, and underground electric power transmission. Natural convection in enclosures is usually characterized by the formation of convective cells due to the buoyancy effect. The heat transfer in enclosures is represented by correlating the average Nusselt number as a function of the Rayleigh number, Prandtl number, and aspect ratio. Enclosures can be classified in two categories: cavity-type and annulus-type.

Natural convection in rectangular and square cavities has been extensively studied by a number of researchers[14-18]. The problem has been tackled experimentally as well as numerically. Both finite-difference[15,16] and finite-element[17] techniques have been used for numerical simulations.

To examine the usefulness and limitations of the present study, a problem of the natural convection in a rectangular cavity has been chosen.

3.1.1 Physical Problem and Mathematical Model

We consider a closed square two-dimensional cavity containing a Newtonian fluid (air) initially at rest at température T_∞ as shown schematically in Figure 3.1. At

time t = 0, the left- and right-hand end walls are instantaneously heated and cooled respectively to temperatures T_h and T_c and thereafter maintained at these temperatures. The upper and lower boundaries are insulated. All surfaces are rigid non-slip boundaries. The Boussinesq approximation is assumed to be valid, which assumes that fluid properties are constant everywhere and the density variation brings about the buoyancy term in momentum equations. The flow is assumed to be laminar and two-dimensional. The subsequent motion is described by the usual equations.

3.1.2 Governing Equations for Laminar Flow

For an incompressible viscous flow of Newtonian fluid the governing continuity and momentum equations can be written as :
continuity

$$\frac{\partial u}{\partial x} + \frac{\partial v}{\partial y} = 0 \tag{3.1}$$

x momentum (note that x is the vertical direction)

$$\rho\frac{\partial u}{\partial t} + \rho(u\frac{\partial u}{\partial x} + v\frac{\partial u}{\partial y}) = -\frac{\partial p}{\partial x} + \mu[\frac{\partial^2 u}{\partial x^2} + \frac{\partial^2 u}{\partial y^2}] - (\rho_\infty - \rho)g \tag{3.2}$$

y momentum

$$\rho\frac{\partial v}{\partial t} + \rho(u\frac{\partial v}{\partial x} + v\frac{\partial v}{\partial y}) = -\frac{\partial p}{\partial y} + \mu[\frac{\partial^2 v}{\partial x^2} + \frac{\partial^2 v}{\partial y^2}] \tag{3.3}$$

Energy

$$\frac{\partial T}{\partial t} + u\frac{\partial T}{\partial x} + v\frac{\partial T}{\partial y} = \alpha[\frac{\partial^2 T}{\partial x^2} + \frac{\partial^2 T}{\partial y^2}] \tag{3.4}$$

where u and v are the vertical and horizontal velocity components in the x and y directions respectively, p is the pressure, T is the temperature, ρ is the density of the fluid, μ is the dynamic viscosity of the fluid, and α is the thermal diffusivity of the fluid. The viscous dissipation effect is neglected in energy equation. It is to be noted that g acts in the x direction.

Following the Boussinesq approximation, density is everywhere constant except in the buoyancy term. The density variation with temperature is stated by the equation

$$\rho_\infty = \rho[1 + \beta(T - T_\infty)] \tag{3.5}$$

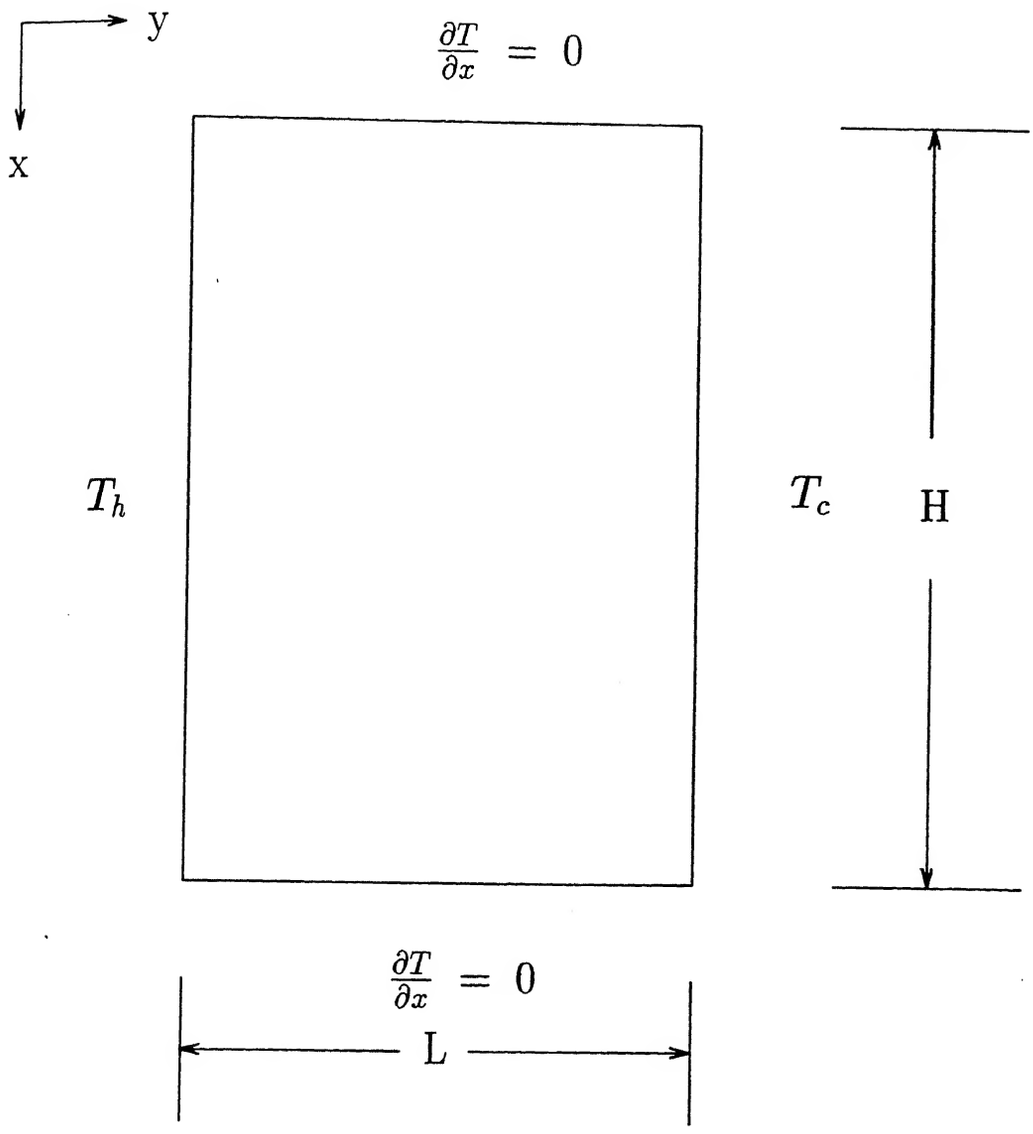

Figure 3.1: Physical configuration and coordinate system.

Therefore

$$(\rho_\infty - \rho) = \rho\beta(T - T_\infty) \tag{3.6}$$

where subscript '∞' stands for the reference state. The parameter β is the coefficient of thermal expansion of the fluid and is given by

$$\beta = -\frac{1}{\rho}(\frac{\partial \rho}{\partial T})_p \tag{3.7}$$

where T is the absolute temperature. For ideal gases, $\beta = 1/T$. After substitution of (3.6) into (3.2) and simplification the x-momentum equation takes the form

$$\rho\frac{\partial u}{\partial t} + \rho(u\frac{\partial u}{\partial x} + v\frac{\partial u}{\partial y}) = -\frac{\partial p}{\partial x} + \mu[\frac{\partial^2 u}{\partial x^2} + \frac{\partial^2 u}{\partial y^2}] - \rho g\beta(T - T_\infty) \tag{3.8}$$

Here the term $g\beta(T - T_\infty)$ represents the buoyancy term. The velocity and the temperature fields are coupled.

The boundary conditions for the present problem are

$$\begin{aligned}
&u = v = 0, && \frac{\partial T}{\partial x} = 0 && on \quad x = 0, && 0 < y < L \\
&u = v = 0, && \frac{\partial T}{\partial x} = 0 && on \quad x = H, && 0 < y < L \\
&u = v = 0, && T = T_h && on \quad y = 0, && 0 \leq x \leq H \\
&u = v = 0, && T = T_c && on \quad y = L, && 0 \leq x \leq H
\end{aligned} \tag{3.9}$$

3.1.3 Non-dimensional Parameters

The problem may be restated in the nondimensional form. We introduce here the following non-dimensional variables

$$U = \frac{uL}{\nu} \qquad V = \frac{vL}{\nu} \qquad X = \frac{x}{L} \qquad Y = \frac{y}{L}$$
$$\tau = \frac{\nu t}{L^2} \qquad \theta = \frac{T - T_c}{T_h - T_c} \qquad P = \frac{(p_\infty - p)L^2}{\rho\nu^2} \qquad Pr = \frac{\nu}{\alpha}$$
$$Gr = \frac{g\beta(T_h - T_c)L^3}{\nu^2}$$

where ν is the kinematic viscosity, Pr is the Prandtl number, and Gr is the Grashof number. It may be mentioned that in this problem T_h has been considered as equivalent to T_w of a general formulation. Similarly, instead of T_∞, we use T_c.

In dimensionless form, the equations are expressed as

$$\frac{\partial U}{\partial X} + \frac{\partial V}{\partial Y} = 0 \tag{3.10}$$

$$\frac{\partial U}{\partial \tau} + U\frac{\partial U}{\partial X} + V\frac{\partial U}{\partial Y} = \frac{\partial P}{\partial X} + [\frac{\partial^2 U}{\partial X^2} + \frac{\partial^2 U}{\partial Y^2}] - \frac{g\beta(T - T_c)L^3}{\nu^2} \tag{3.11}$$

$$\frac{\partial V}{\partial \tau} + U\frac{\partial V}{\partial X} + V\frac{\partial V}{\partial Y} = \frac{\partial P}{\partial Y} + [\frac{\partial^2 V}{\partial X^2} + \frac{\partial^2 V}{\partial Y^2}] \tag{3.12}$$

$$\frac{\partial \theta}{\partial \tau} + U\frac{\partial \theta}{\partial X} + V\frac{\partial \theta}{\partial Y} = \frac{1}{Pr}[\frac{\partial^2 \theta}{\partial X^2} + \frac{\partial^2 \theta}{\partial Y^2}] \tag{3.13}$$

The boundary conditions for the problem in nondimensional form are given by

$$\begin{aligned}
U &= V = 0, \quad \frac{\partial \theta}{\partial X} = 0 \quad on \quad X = 0, \quad 0 < Y < 1 \\
U &= V = 0, \quad \frac{\partial \theta}{\partial X} = 0 \quad on \quad X = Ar, \quad 0 < Y < 1 \\
U &= V = 0, \quad \theta = 1 \quad on \quad Y = 0, \quad 0 \leq X \leq Ar \\
U &= V = 0, \quad \theta = 0 \quad on \quad Y = 1, \quad 0 \leq X \leq Ar
\end{aligned} \tag{3.14}$$

where Ar = H/L is the aspect ratio.

The conservation of the mass, momentum, and energy governing the buoyancy driven fluid flow and heat transfer in the enclosure may be formulated in terms of dimensionless quantities of stream function, vorticity, and temperature, respectively. For two-dimensional problem, it is convenient to define a stream function ψ and vorticity ω as

$$U = \frac{\partial \psi}{\partial Y} \qquad V = -\frac{\partial \psi}{\partial X} \tag{3.15}$$

$$\omega = \frac{\partial V}{\partial X} - \frac{\partial U}{\partial Y} \tag{3.16}$$

We can readily see that existence of (3.15) automatically satisfies continuity equation (3.10). If we substitute the dependent variable with stream function, we shall not be concerned with equation (3.10) any more. Invoking equation (3.15) into (3.16) we obtain Poisson equation

$$\frac{\partial^2 \psi}{\partial X^2} + \frac{\partial^2 \psi}{\partial Y^2} = -\omega \tag{3.17}$$

Table 3.1: Expressions for parameters in general transport equation

Function	ϕ	Λ	Γ	S_ϕ
Temperature	θ	1	$\frac{1}{Pr}$	0
Vorticity	ω	1	1	$Gr\frac{\partial\theta}{\partial Y}$
Stream function	ψ	0	1	ω

Now we differentiate equation (3.11) with respect to Y and equation (3.12) with respect to X. If we subtract differentiated equation (3.12) from differentiated equation (3.11) and rearrange the resulting equation, we shall obtain

$$\frac{\partial\omega}{\partial\tau}+U\frac{\partial\omega}{\partial X}+V\frac{\partial\omega}{\partial Y}=[\frac{\partial^2\omega}{\partial X^2}+\frac{\partial^2\omega}{\partial Y^2}]+Gr\frac{\partial\theta}{\partial Y} \tag{3.18}$$

This equation is the vorticity transport equation.

Instead of solving Poisson equation for stream function, we solve the Cauchy Kowaleska equation, i.e., the Poisson equation is recast in a false transient form as a solution strategy.

$$\frac{\partial\psi}{\partial\tau}=\frac{\partial^2\psi}{\partial X^2}+\frac{\partial^2\psi}{\partial Y^2}+\omega \tag{3.19}$$

The equations (3.13),(3.18), and (3.19) are the governing differential equations for two dimensional natural convection problems with moderate buoyancy effects. The vorticity equation is coupled to the parabolic Cauchy Kowaleska equation through the nonlinear convection terms and the energy equation is coupled to the vorticity equation. These dimensionless equations for vorticity, stream function and temperature can be represented by the following general transport equation in terms of the flow property ϕ

$$\frac{\partial\phi}{\partial\tau}+\Lambda(U\frac{\partial\phi}{\partial X}+V\frac{\partial\phi}{\partial Y})=\Gamma[\frac{\partial^2\phi}{\partial X^2}+\frac{\partial^2\phi}{\partial Y^2}]+S_\phi \tag{3.20}$$

where S_ϕ is a source term, Γ is a diffusion coefficient, and β is a constant. The parameters used in general transport equation (3.20) are defined in Table 3.1.

The boundary conditions to be satisfied by stream function, vorticity, and temperature are shown in the Table 3.2.

The advantage of stream function vorticity formulation is that the pressure gets eliminated from momentum equations and we solve only two equations, one for stream function and other for vorticity, instead of solving three equations, one continuity and

Table 3.2: Expressions for boundary conditions for natural convection in rectangular cavity

Function	ϕ	Top wall	Bottom wall	Left wall	Right wall
Temperature	θ	$\frac{\partial\theta}{\partial X}=0$	$\frac{\partial\theta}{\partial X}=0$	$\theta=1$	$\theta=0$
Vorticity	ω	$\omega=-\frac{\partial^2\psi}{\partial X^2}$	$\omega=-\frac{\partial^2\psi}{\partial X^2}$	$\omega=-\frac{\partial^2\psi}{\partial Y^2}$	$\omega=-\frac{\partial^2\psi}{\partial Y^2}$
Stream function	ψ	ψ *or* $\frac{\partial\psi}{\partial X}=0$	ψ *or* $\frac{\partial\psi}{\partial X}=0$	ψ *or* $\frac{\partial\psi}{\partial Y}=0$	ψ *or* $\frac{\partial\psi}{\partial Y}=0$

two momentum equations. However, the approach is not free from computational difficulties. In solution of vorticity equation, the first difficulty arises from the boundary conditions, since the vorticity is unknown along boundaries. The method generally employed is that the stream function equation is used at the wall in order to generate Dirichlet-type conditions. The second difficulty that arises is due to the variation of these boundary conditions at each time step.

At no-slip boundaries, vorticity is produced. The boundary conditions for ω are obtained using the no-slip condition at the wall and expression (3.17). Let us consider X = 0 wall, where

$$\omega=-\frac{\partial^2\psi}{\partial X^2}, \qquad \frac{\partial\psi}{\partial X}=0 \qquad and \quad \psi=0 \tag{3.21}$$

We use finite-difference technique to compute vorticity at the wall. Applying central difference at a point 'b' on the wall, we get

$$\omega_{ub}=-\frac{\psi_{ub+1}-2\psi_{ub}+\psi_{ub-1}}{\Delta X^2} \tag{3.22}$$

$$and \qquad \frac{\psi_{ub+1}-\psi_{ub-1}}{2\Delta X}=\psi_{ub}=0$$

where the suffix 'ub' stands for upper boundary. After simplification we get

$$\omega_{ub}=-\frac{2\psi_{ub+1}}{\Delta X^2} \tag{3.23}$$

In a similar fashion, we get

$$at \qquad X=Ar, \qquad \omega_{bb}=-\frac{2\psi_{bb-1}}{\Delta X^2} \tag{3.24}$$

$$at \qquad Y=0, \qquad \omega_{lb}=-\frac{2\psi_{lb+1}}{\Delta Y^2}$$

$$at \qquad Y=1, \qquad \omega_{rb}=-\frac{2\psi_{rb-1}}{\Delta Y^2}$$

subscripts 'bb', 'lb', and 'rb' represents bottom, left, and right walls respectively.

The rate of heat transfer along each wall is determined from the temperature field. The local Nusselt number along the heated wall is

$$Nu = -\frac{\partial\theta}{\partial Y}|_{Y=0} \tag{3.25}$$

The average value of the Nusselt number is evaluated using

$$\overline{Nu} = -\frac{1}{Ar}\int_0^{Ar}(\frac{\partial\theta}{\partial Y})_{Y=0}dX \tag{3.26}$$

The derivative $\frac{\partial\theta}{\partial Y}$ is computed by using spectral element technique. We compute the integration in equation (3.26) by the trapezoidal rule.

$$\overline{Nu} = \frac{1}{2Ar}\sum_{i=1}^{N_x e_x+1}[\Delta X_i(Nu_i + Nu_{i+1})] \tag{3.27}$$

where Nu_i is the Nusselt number at the i^{th} point and $\Delta X_i = X_{i+1} - X_i$. $N_x e_x + 1$ represents the total number of points in x-direction. The domain is assumed to consist of e_x elements in this direction.

3.1.4 Discretization and Solution Procedure

The governing equations are unsteady, coupled, non-linear partial differential equations, for which a semi-implicit scheme is used for time discretization. As already stated in chapter 2, the non-linear convection terms are treated explicitly while the diffusion term implicitly. The time discretized form of the governing equations for temperature, stream function and vorticity is given by the well known Helmholtz equation of the form

$$\phi_{xx} + \phi_{yy} - \lambda_\phi^2\phi = f_\phi \tag{3.28}$$

Where the parameter λ_ϕ^2 and the forcing function f_ϕ for temperature, stream function and vorticity transport equations are defined in Table 3.3

The spectral element method is used for spatial discretization, in which the variable ϕ is expressed in terms of Lagrangian interpolant through Gauss-Lobatto Chebyshev collocation points, which are closely spaced near the elemental boundaries. This method uses variational approach which requires that the functional is to be maximized. Maximization of functional results in the elemental equations, defined in chapter 2. These equations are combined to form the global set which is expressed as

$$C_{p_g q_g}^{global}\phi_{q_g}^{global} = e_{p_g}^{global} \tag{3.29}$$

where p_g and q_g are the global indices, expressed by

Table 3.3: Expressions for λ_ϕ^2 and forcing function f_ϕ

Equation	ϕ	λ_ϕ^2	f_ϕ
Energy	θ	$\frac{Pr}{\Delta\tau}$	$-\frac{\theta^n}{\Delta\tau/Pr} + Pr[U\frac{\partial\theta}{\partial X} + V\frac{\partial\theta}{\partial Y}]^n$
Vorticity transport	ω	$\frac{1}{\Delta\tau}$	$-\frac{\omega^n}{\Delta\tau} + [U\frac{\partial\omega}{\partial X} + V\frac{\partial\omega}{\partial Y}]^n - Gr(\frac{\partial\theta}{\partial Y})^n$
Stream function	ψ	$\frac{1}{\Delta\tau}$	$-(\frac{\psi^n}{\Delta\tau} + \omega^n)$

$$p_g = 1, 2, ..., (N_x e_x + 1)(N_y e_y + 1)$$
$$q_g = 1, 2, ..., (N_x e_x + 1)(N_y e_y + 1)$$

and f_q is the known forcing function which changes at each time step. The solution procedure used to obtain the steady state solution is described as follows:

1. Specify the initial guess for the temperature, vorticity, stream function, and velocities.
2. Solve the energy equation at n+1 time step.
3. Solve the vorticity equation at n+1 time step.
4. Solve the Cauchy Kowaleska equation for the stream function at n+1 time step.
5. Compute the velocity field in the solution domain and vorticity at the boundaries.
6. Check the convergence by the criterion

$$rms = \sqrt{\frac{\sum_{i=1}^{N_{total}} [\phi_i^{n+1} - \phi_i^n]^2}{N_{total}}} < \epsilon \tag{3.30}$$

Where ϵ is the preassigned tolerance value, and *rms* is the rms difference value, defined as the square root of the average of the squares of the differences between two successive time step values.

The procedure is repeated until the convergence condition Eq.(3.30) is satisfied.

The spectral element method has two ways to achieve better numerical accuracy, i.e., by increasing the nodes in the elements, and/or increasing the number of elements. The optimum choice of these two parameters depends on each individual problem to be solved. Without changing the total number of the interpolation points, using more elements in each direction reduces the computational cost, but at the same time, the accuracy level becomes lower.

3.2 Natural Convection Heat Transfer in a Vertical Rectangular Enclosure with Discrete Heating

The ever-increasing demand for faster and smaller computer elements has led to the development of compact electronic equipments of high heat dissipation rates per unit area [21]. Typically, the power density of ceramic chip carriers is about 500 KW/m^2, and the maximum temperature allowed is approximately 100^0 C or less. For safe and reliable working of these densely packed electronic components proper cooling is essential to limit the operative temperature. Out of various cooling methods, natural cooling by free convection plays an important role in many electronic packages. Cooling by natural convection is preferred because of its high reliability, absence of noise, and low maintenance cost. Under certain circumstances, such as operation of electronic equipment in dusty or hazardous environment, electronic equipments are packed within sealed enclosures. The components may be mounted to one vertical wall of the enclosure, while one or more of the other walls is cooled.

3.2.1 Physical Problem and Mathematical Model

For the purpose of numerical study, we consider the natural convection cooling of discrete fluish-mounted heaters inside a vertical rectangular enclosure [19], as shown schematically in Figure 3.2. A vertical rectangular enclosure with four discrete fluish-mounted heat sources of isoflux q_h on the left vertical wall is considered. The discrete heaters of length l are placed at an equal spacing s between the fixed adiabatic top and bottom surfaces of the enclosure. The right vertical wall of the enclosure is isothermally cooled at temperature T_c.

The following assumptions are made:

- Two-dimensional laminar flow and heat transfer.
- The fluid (air) within the enclosure is considered to be Newtonian.
- The physical properties, such as viscosity, thermal conductivity, etc., are assumed to be independent of temperature except for the density, in the buoyancy term in momentum equations, that is assumed temperature dependent. (Boussinesq approximation)

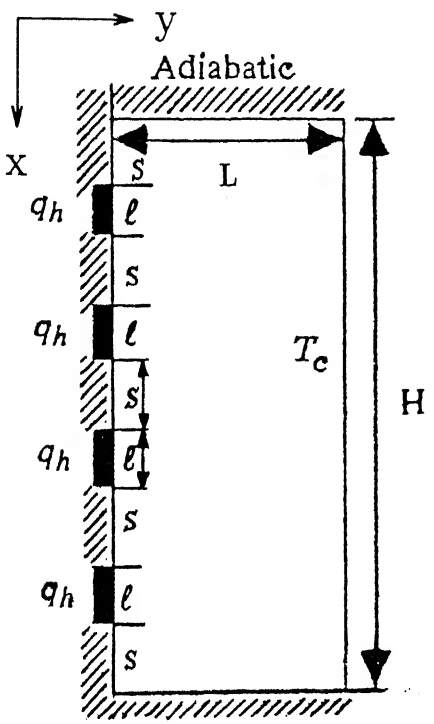

Figure 3.2: Physical configuration and coordinate system

With the assumptions stated above, the governing equations for buoyancy driven fluid flow and heat transfer in the enclosure, in terms of stream function, vorticity, and temperature are as follows

$$\frac{\partial\theta}{\partial\tau} + U\frac{\partial\theta}{\partial X} + V\frac{\partial\theta}{\partial Y} = \frac{1}{Pr}[\frac{\partial^2\theta}{\partial X^2} + \frac{\partial^2\theta}{\partial Y^2}] \tag{3.31}$$

$$\frac{\partial\omega}{\partial\tau} + U\frac{\partial\omega}{\partial X} + V\frac{\partial\omega}{\partial Y} = [\frac{\partial^2\omega}{\partial X^2} + \frac{\partial^2\omega}{\partial Y^2}] + Gr^*\frac{\partial\theta}{\partial Y} \tag{3.32}$$

$$\frac{\partial\psi}{\partial\tau} = \frac{\partial^2\psi}{\partial X^2} + \frac{\partial^2\psi}{\partial Y^2} + \omega \tag{3.33}$$

with the boundary conditions:

$$\begin{aligned}
\psi &= 0, \quad \frac{\partial\theta}{\partial Y} = -1 \quad (at\ heaters) \quad Y = 0, \\
&\quad \frac{\partial\theta}{\partial Y} = 0 \quad (elsewhere) \\
\psi &= 0, \quad \theta = 0 \quad Y = 1 \\
\psi &= 0, \quad \frac{\partial\theta}{\partial X} = 0 \quad on \quad X = 0, \\
\psi &= 0, \quad \frac{\partial\theta}{\partial X} = 0 \quad on \quad X = Ar,
\end{aligned} \tag{3.34}$$

where Ar is the aspect ratio (= H/L) is the aspect ratio, Gr^* is the modified Grashof number defined as $Gr^* = \frac{g\beta q_h L^4}{k\nu^2}$.

The local heat transfer rates at the discretely heated wall and the isothermally cold wall are estimated by the knowledge of local Nusselt numbers defined as follows

$$Nu_h = \frac{1}{\theta_h} \tag{3.35}$$

$$Nu_c = -(\frac{\partial\theta}{\partial Y})_{Y=1} \tag{3.36}$$

3.3 Flow Analysis in Vertical Fin Arrays

Vertical fins are widely used in the cooling of electronic devices. A numerical investigation for predicting the heat transfer from the vertical fins have been reported by Sukhatme and Saikhedkar [22]. Present study uses a similar geometrical configuaration for the Spectral Element Method. Essentially, the problem is concerned with vertical fin arrays which are attached on a hot base with temperature T_w. The fins transfer heat to the surrounding fluid by natural convection. The vertical fin arrays to be analysed are shown in Figure 3.3. It consists of a large number of rectangular fins of a small thickness projected out from a common vertical base plate. Two adjacent fins and the base plate constitute a channel through which natural convective flow takes place. Due to the geometrical symmetry, the rectangular channel formed by the ABCD and EFGH planes form the domain of primary interest. However, because of the fact that the fins are situated in an otherwise quiescent environment which is influenced by the fin temperature, the analytical domain is extended and a rectangular channel between the planes KLMN and PQRS becomes the configuration of interest. The distribution of elements on each vertical plane is same and one such typical distribution on KLMN plane has been shown in Figure 3.4. The shaded area indicates the location of the fin.

3.3.1 Physical Problem and Mathematical Model

As mentioned earlier, a series of fins of height H in x-direction, length L in y-direction and the spacing $2B$ in z-direction are attached to the hot base which is maintained at uniform temperature T_w. The solid surface and the fins constitute a part of the computational domain. Heat is transferred from the solid base of uniform temperature to fins by conduction and to infinite ambient fluid of temperature T_∞ by natural convection.

Let x denotes vertical coordinate direction, y denotes the coordinate perpendicular to the wall, and z coordinate is in the direction of successive fins. The gravitational field acts in x direction. The fluid flow is assumed to be essentially two dimensional with velocity components u and v being in x and y directions respectively. Cross flow in z direction is negligible in magnitude. Instead, it is assumed that the diffusion occurs in all the three directions. This simplified assumption of two dimensional flow allows us to use stream function vorticity formulation. Flow is considered to be laminar, further it is assumed that there is no viscous dissipation. The usual

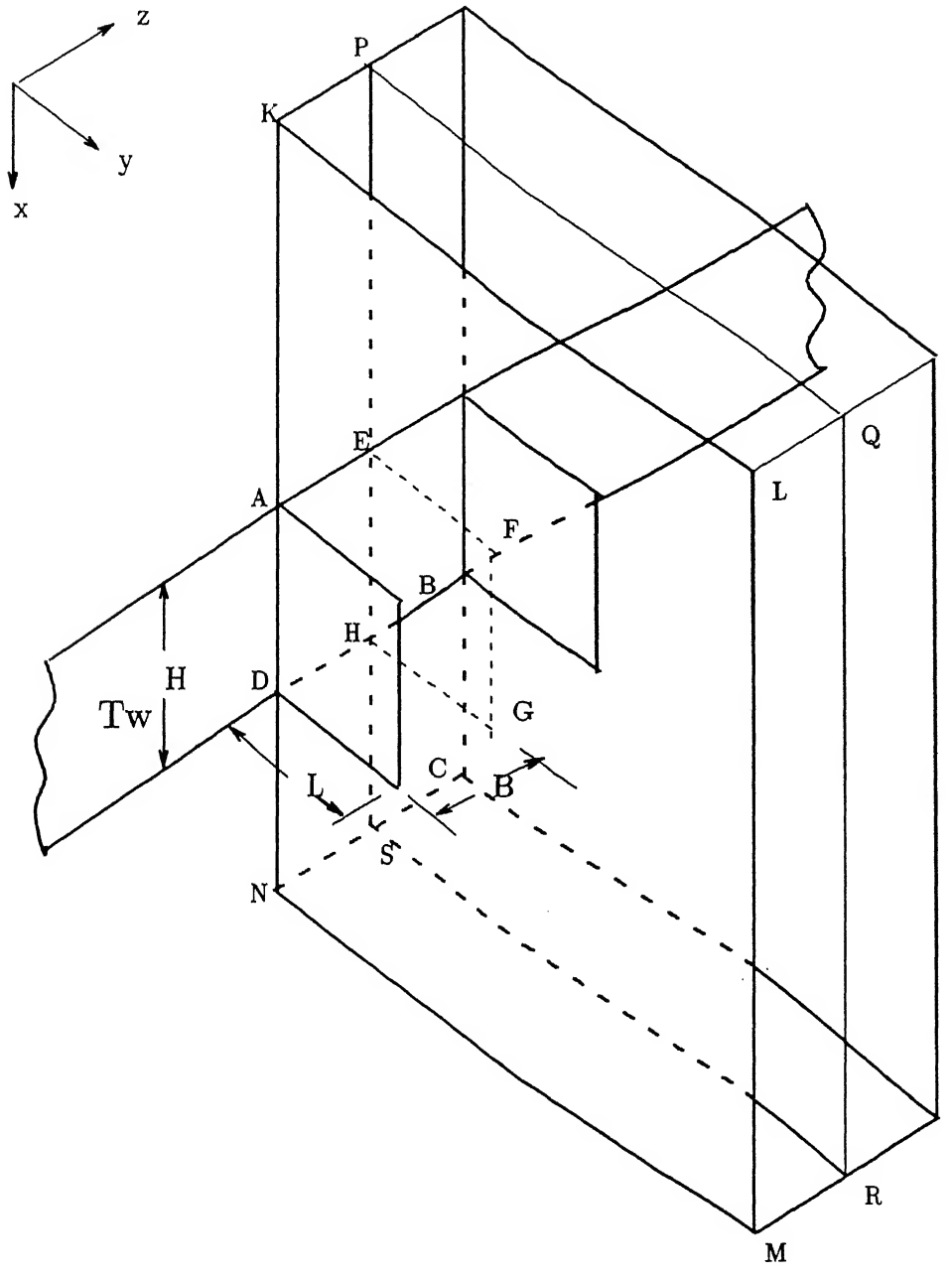

Figure 3.3: Physical configuration and coordinate system.

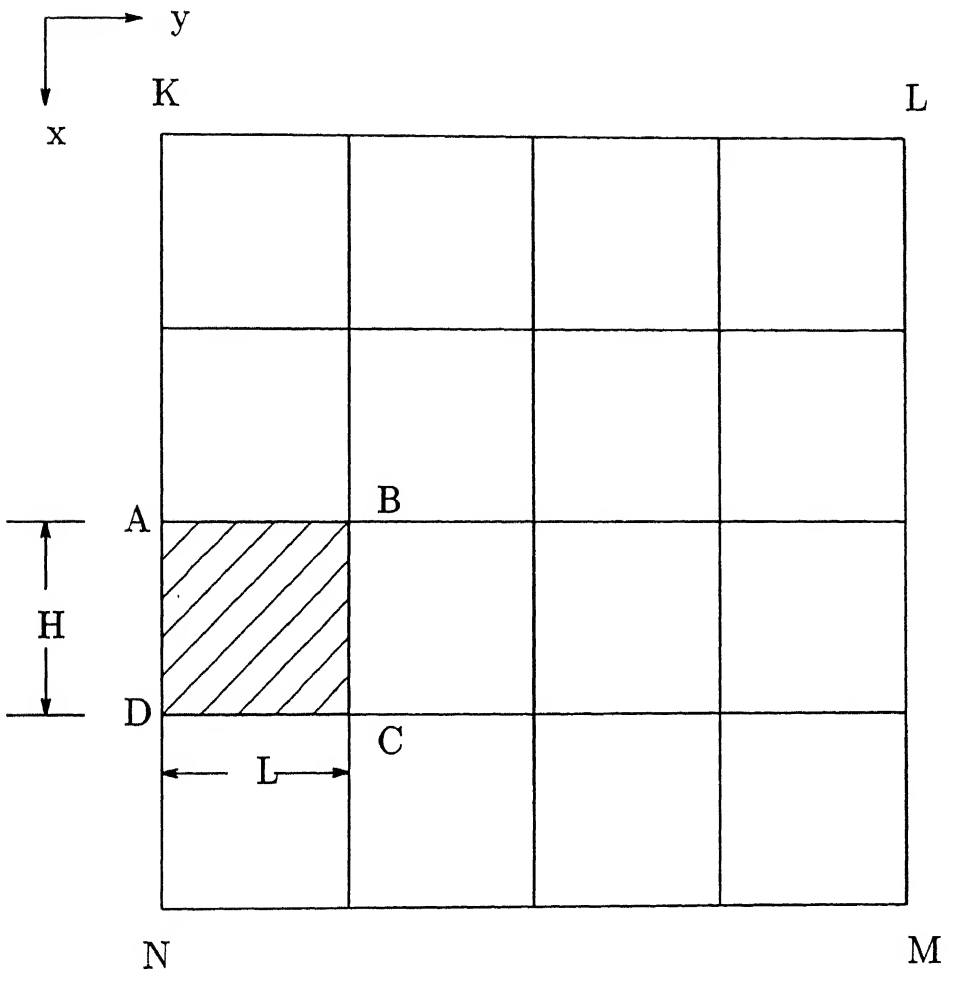

Figure 3.4: Location of the fin on a x-y plane.

Boussinesq approximation is assumed to be valid. The governing equations that describe this problem are the Navier-Stokes and energy equations.

For an incompressible flow of a Newtonian fluid, the governing equations, incorporating the above mentioned assumptions, are as follows:
continuity

$$\frac{\partial u}{\partial x} + \frac{\partial v}{\partial y} = 0 \tag{3.37}$$

x momentum

$$\rho\frac{\partial u}{\partial t} + \rho(u\frac{\partial u}{\partial x} + v\frac{\partial u}{\partial y}) = -\frac{\partial p}{\partial x} + \mu[\frac{\partial^2 u}{\partial x^2} + \frac{\partial^2 u}{\partial y^2} + \frac{\partial^2 u}{\partial z^2}] - \rho g\beta(T - T_\infty) \tag{3.38}$$

y momentum

$$\rho\frac{\partial v}{\partial t} + \rho(u\frac{\partial v}{\partial x} + v\frac{\partial v}{\partial y}) = -\frac{\partial p}{\partial y} + \mu[\frac{\partial^2 v}{\partial x^2} + \frac{\partial^2 v}{\partial y^2} + \frac{\partial^2 v}{\partial z^2}] \tag{3.39}$$

Energy

$$\frac{\partial T}{\partial t} + u\frac{\partial T}{\partial x} + v\frac{\partial T}{\partial y} = \alpha[\frac{\partial^2 T}{\partial x^2} + \frac{\partial^2 T}{\partial y^2} + \frac{\partial^2 T}{\partial z^2}] \tag{3.40}$$

where u and v are the vertical and horizontal velocity components, T_∞ is the temperature of the quiescent ambient fluid, μ is the dynamic viscosity and α is the thermal diffusivity of the fluid considered. Except for ρ in the buoyancy term in x momentum equation, the fluid properties are assumed constants. The dependence of density on temperature is related by

$$\rho_\infty = \rho[1 + \beta(T - T_\infty)] \tag{3.41}$$

In the above equation, constant β stands for the volume coefficient of thermal expansion of the fluid.

3.3.2 Non-dimensional Parameters

To represent the problem in non-dimensional form the following nondimensional parameters are introduced

$$U = \frac{uH}{\nu} \qquad V = \frac{vH}{\nu} \qquad X = \frac{x}{H} \qquad Y = \frac{y}{H} \qquad Z = \frac{z}{H}$$
$$\tau = \frac{\nu t}{H^2} \qquad \theta = \frac{T - T_\infty}{T_w - T_\infty} \qquad P = \frac{(p_\infty - p)H^2}{\rho\nu^2} \qquad Pr = \frac{\nu}{\alpha}$$

$$Gr = \frac{g\beta(T_W - T_\infty)H^3}{\nu^2}$$

Here H is the height of the fin, p_∞ is the reference pressure at reference temperature T_∞, ν is the kinematic viscosity and Pr is the Prandtl number of the fluid. Gr_H is the Grashof number based on the height of the fin.

The governing equations for conservation of mass, momentum, and energy are nondimensionalized using these non-dimensional parameters. In non-dimensional form these equations are given by

$$\frac{\partial U}{\partial X} + \frac{\partial V}{\partial Y} = 0 \tag{3.42}$$

$$\frac{\partial U}{\partial \tau} + U\frac{\partial U}{\partial X} + V\frac{\partial U}{\partial Y} = \frac{\partial P}{\partial X} + [\frac{\partial^2 U}{\partial X^2} + \frac{\partial^2 U}{\partial Y^2} + \frac{\partial^2 U}{\partial Z^2}] - Gr_H\theta \tag{3.43}$$

$$\frac{\partial V}{\partial \tau} + U\frac{\partial V}{\partial X} + V\frac{\partial V}{\partial Y} = \frac{\partial P}{\partial Y} + [\frac{\partial^2 V}{\partial X^2} + \frac{\partial^2 V}{\partial Y^2} + \frac{\partial^2 V}{\partial Z^2}] \tag{3.44}$$

$$\frac{\partial \theta}{\partial \tau} + U\frac{\partial \theta}{\partial X} + V\frac{\partial \theta}{\partial Y} = \frac{1}{Pr}[\frac{\partial^2 \theta}{\partial X^2} + \frac{\partial^2 \theta}{\partial Y^2} + \frac{\partial^2 \theta}{\partial Z^2}] \tag{3.45}$$

There are two basic approaches for numerical solution of these equations: primitive variables approach and stream function vorticity approach. The primitive variables approach considers the above equations directly, taking the velocity components and the pressure. The stream function and vorticity approach employs derived variables, namely, stream function and vorticity to solve the problem. As a consequence the pressure gets eliminated and the existence of stream function identically satisfies the continuity equation.

We have already defined vorticity ω as

$$\omega = \frac{\partial V}{\partial X} - \frac{\partial U}{\partial Y} \tag{3.46}$$

If we define stream function in two-dimensional plane as $\psi = \psi(X, Y)$, then

$$U = \frac{\partial \psi}{\partial Y} \qquad V = -\frac{\partial \psi}{\partial X} \tag{3.47}$$

which culminates in

$$\frac{\partial^2 \psi}{\partial X^2} + \frac{\partial^2 \psi}{\partial Y^2} = -\omega \tag{3.48}$$

The false transient form of equation (3.48) is given by

$$\frac{\partial \psi}{\partial \tau} = \frac{\partial^2 \psi}{\partial X^2} + \frac{\partial^2 \psi}{\partial Y^2} + \omega \tag{3.49}$$

Elimination of pressure from momentum equations results in the following vorticity transport equation

$$\frac{\partial \omega}{\partial \tau} + U\frac{\partial \omega}{\partial X} + V\frac{\partial \omega}{\partial Y} = [\frac{\partial^2 \omega}{\partial X^2} + \frac{\partial^2 \omega}{\partial Y^2} + \frac{\partial^2 \omega}{\partial Z^2}] + Gr_H \frac{\partial \theta}{\partial Y} \tag{3.50}$$

We note from the above equations that the Grashof and Prandtl numbers are the two governing parameters for the problem of interest.

All these equations for vorticity, stream function, and temperature can be represented by the general equation of the form

$$\frac{\partial \phi}{\partial \tau} + \Lambda(U\frac{\partial \phi}{\partial X} + V\frac{\partial \phi}{\partial Y}) = \Gamma[\frac{\partial^2 \phi}{\partial X^2} + \frac{\partial^2 \phi}{\partial Y^2} + \frac{\partial^2 \phi}{\partial Z^2}] + S_\phi \tag{3.51}$$

where meaning of terms is explained in Table 3.1.

3.3.3 Boundary Conditions for Present Problem

The relevant boundary conditions for the problem are as follows:

- At the fin base surface AEHD ($2H \leq x \leq 3H, 0 \leq z \leq B, y = 0$) (solid surface)

  The no slip boundary condition and the prescribed wall temperature is

  $u = v = 0 \qquad \psi = 0 \qquad T = T_w$

  $\frac{\partial v}{\partial x} = 0, \qquad \omega = -\frac{\partial u}{\partial y} = -\frac{\partial^2 \psi}{\partial y^2}$

- At the top extension of fin base surface AEPK ($0 \leq x \leq 2H, 0 \leq z \leq B, y = 0$)

  $\omega = 0 \qquad \psi = 0 \qquad \frac{\partial T}{\partial y} = 0$

- At the bottom extension of fin base surface DHSN ($3H \leq x \leq 4H, 0 \leq z \leq B, y = 0$)

  $\frac{\partial \omega}{\partial y} = 0, \qquad \frac{\partial \psi}{\partial y} = 0, \qquad \frac{\partial T}{\partial y} = 0$

- At the surface ABCD, z = 0

  symmetry conditions give

  $\frac{\partial \omega}{\partial z} = 0,$

  $u = v = 0, \qquad \psi = 0$

- At the vertical mid fin channel section PQRS $z = B$ symmetry conditions requires

$$\frac{\partial u}{\partial z} = 0, \qquad \frac{\partial v}{\partial z} = 0, \qquad \frac{\partial \omega}{\partial z} = 0, \qquad \frac{\partial T}{\partial z} = 0,$$

- At the surface LQRM

$$\frac{\partial T}{\partial y} = 0, \qquad \frac{\partial \omega}{\partial y} = 0, \qquad \frac{\partial \psi}{\partial y} = 0,$$

- At the surface KLMNDCBA (z = 0)

$$\frac{\partial u}{\partial z} = 0, \qquad \frac{\partial v}{\partial z} = 0, \qquad \frac{\partial T}{\partial z} = 0, \qquad \frac{\partial \omega}{\partial z} = 0,$$

The mass, momentum and energy conservation equations discussed above are the fundamental equations for natural convection in the geometry shown in Figure 3.3. The basic mechanism by which heat is transferred to the fins attached to surface is conduction. The fins are assumed to be very thin, equal to the thickness of the plane, and that the heat transfer from the fin boundaries is neglected. Instead, heat is transferred from the fin surfaces to ambient fluid in z direction. The temperature distribution in fin (solid) is governed by the transient heat conduction equation given by

$$\rho_s c_s \frac{\partial T_s}{\partial t} = k_s[\frac{\partial^2 T_s}{\partial x^2} + \frac{\partial^2 T_s}{\partial y^2}] + \frac{k}{\delta}\frac{\partial T}{\partial z} \tag{3.52}$$

where T_s is the temperature in the fin (solid), ρ_s, c_s and k_s refer to the density, specific heat and thermal conductivity of the fin, δ is the half thickness of the fin, and k is the thermal conductivity of the fluid. The second term on the right side of equation (3.52) expresses the heat loss from fin surface to the adjacent fluid on its either side.

The boundary conditions along the fin boundaries can be taken as

$$\begin{aligned}
T_s &= T_w \qquad 2H \le x \le 3H, \quad y = 0 \\
\frac{\partial T_s}{\partial x} &= 0 \qquad on \quad x = 2H, \quad 0 < y \le L \\
\frac{\partial T_s}{\partial y} &= 0 \qquad on \quad 2H \le x \le 3H, \quad y = L \\
\frac{\partial T_s}{\partial x} &= 0 \qquad on \quad x = 3H, \quad 0 < y \le L
\end{aligned} \tag{3.53}$$

alongwith the initial condition $T_s = T_{s0}$ for $t \le 0$.

Since the energy equation (3.52) is essentially for the fin material, it is nondimensionalized separately. Here x, y, z and t are nondimensionalized in the same

way described earlier. Employing the nondimensionalization of T_s in terms of reference temperature T_∞ as $\theta_s = (T_s - T_\infty)/(T_w - T_\infty)$, the governing equation (3.52) is obtained in dimensionless terms, given by

$$\frac{\partial \theta_s}{\partial \tau} = \frac{\alpha_s}{\alpha}\frac{1}{Pr}\left[\frac{\partial^2 \theta_s}{\partial X^2} + \frac{\partial^2 \theta_s}{\partial Y^2}\right] + \frac{1}{\mathrm{Pr}}\frac{\rho c}{\rho_s c_s}\frac{H}{\delta}\frac{\partial \theta}{\partial Z} \tag{3.54}$$

together with the initial and boundary conditions

$$\begin{aligned} \theta_s &= \theta_{s0} \qquad for \quad \tau \leq 0 \\ \theta_s &= 1 \qquad 2 \leq X \leq 3, \quad Y = 0 \quad \tau > 0 \\ \frac{\partial \theta_s}{\partial X} &= 0 \qquad on \quad X = 2, \quad 0 < Y \leq L/H \\ \frac{\partial \theta_s}{\partial Y} &= 0 \qquad on \quad 2 \leq X \leq 3, \quad Y = L/H \\ \frac{\partial \theta_s}{\partial X} &= 0 \qquad on \quad X = 3, \quad 0 < Y \leq L/H \end{aligned} \tag{3.55}$$

where α_s and α are the thermal diffusivities of solid and fluid respectively, ν is the kinematic viscosity and Pr is the Prandtl number of the fluid. $\partial\theta/\partial Z$ is the temperature gradient in z direction.

The above formulation suggests that the heated surface is cooled by free convection to the ambient fluid and by conducting heat to the fins which, in turn, convect heat to the ambient fluid. The convective heat transfer coefficient can be presented in terms of the local Nusselt number Nu, which is defined as $Nu = \frac{hS}{k}$. Also the local heat transfer coefficient h may be expressed in terms of the temperature gradient at the surface, ambient temperature and surface temperature. Thus

$$Nu = \frac{hS}{k} = \frac{-(\frac{\partial T}{\partial n})_w}{T_w - T_\infty} S = \frac{q_{conv} S}{T_w - T_\infty} k \tag{3.56}$$

Here, the subscript w represents the relevant wall or surface, k stands for the thermal conductivity of the fluid and $\frac{\partial T}{\partial n}$ is the temperature gradient normal to the surface.

The mean Nusselt number $\overline{Nu}$ for the surface is defined as $\overline{Nu} = \frac{\bar{h}S}{k}$, where

$$\overline{Nu} = \frac{1}{A}\int_A Nu dA = \frac{1}{S}\int_S Nu ds \tag{3.57}$$

In above relation for average Nusselt number, 'A' is the total surface area exposed to the fluid and S is the distance along the surface.

The local Nusselt number at the fin surface, in terms of nondimensional quantities, is expressed as

$$Nu(X, Y) = -\frac{\partial \theta}{\partial Z} \tag{3.58}$$

We use the second-order Taylor expansion to approximate the derivative of θ on the surface. The resulting expression is given by

$$Nu(X,Y) = -\frac{3\theta_k + 4\theta_{k+1} - \theta_{k+2}}{2\Delta Z} \tag{3.59}$$

The spanwise average Nusselt number distribution on the surface, $\overline{Nu}_{s,X}$, is given by

$$\begin{aligned} \overline{Nu}(s,X) &= \frac{1}{L/H}\int_0^{L/H} Nu(X,Y)dY \\ &= \frac{1}{2L/H}\sum_{j=1}^{N_y.e_y+1}[\Delta Y_j(Nu_{i,j} + Nu_{i,j+1})] \end{aligned} \tag{3.60}$$

and the area averaged Nusselt number, based on the area of the fin surface, is obtained from

$$\begin{aligned} \overline{Nu}(s,a) &= \int_0^1 \overline{Nu}(s,X)dX \\ &= \frac{1}{2}\sum_{i=1}^{N_x.e_x+1}[\Delta X_i(\overline{Nu}_i + \overline{Nu}_{i+1})] \end{aligned} \tag{3.61}$$

3.3.4 Discretization and Solution Procedure

Solution for a three-dimensional flow problem requires considerable effort. However, with some simplifications the problem can be dealt easily.

Comparison with the two-dimensional problem shows the presence of one additional diffusion term $\frac{\partial^2\phi}{\partial Z^2}$ in governing equations. This term, along with non linear convective and source terms, is treated explicitly and the two-dimensional diffusion in x and y directions implicitly. This treatment enables us to adopt the same spatial discretization discussed in chapter 2 with only one difference of inclusion of this additional term in forcing function. To simplify the analysis further, the finite difference scheme is used to approximate all the derivatives in z direction and the problem is solved for successive planes in this direction.

The time discretized form of the equation (3.51) is given by

$$\frac{\phi^{n+1} - \phi^n}{\Gamma\Delta\tau} + \frac{\Lambda}{\Gamma}\left[U\frac{\partial\phi}{\partial X} + V\frac{\partial\phi}{\partial Y}\right]^n = \left[\frac{\partial^2\phi}{\partial X^2} + \frac{\partial^2\phi}{\partial Y^2}\right]^{n+1} + \left[\frac{\partial^2\phi}{\partial Z^2}\right]^n + \frac{S_\phi^n}{\Gamma} \tag{3.62}$$

this can be rearranged as

$$\left(\frac{\partial^2\phi}{\partial X^2}\right)^{n+1} + \left(\frac{\partial^2\phi}{\partial Y^2}\right)^{n+1} - \frac{\phi^{n+1}}{\Gamma\Delta\tau} = -\frac{\phi^n}{\Gamma\Delta\tau} + \frac{\Lambda}{\Gamma}\left[U\frac{\partial\phi}{\partial X} + V\frac{\partial\phi}{\partial Y}\right]^n - \left[\frac{\partial^2\phi}{\partial Z^2}\right]^n - \frac{S_\phi^n}{\Gamma} \tag{3.63}$$

Table 3.4: Expressions for λ_ϕ^2 and forcing function f_ϕ

Equation	ϕ	λ_ϕ^2	f_ϕ
Energy (1)	θ_s	$\frac{\alpha Pr}{\alpha_s \Delta\tau}$	$-\frac{\alpha Pr \theta_s^n}{\alpha_s \Delta\tau} + \frac{\alpha}{\alpha_s}\frac{\rho c}{\rho_s c_s}\frac{H}{\delta}(\frac{\partial\theta}{\partial Z})^n$
Energy (2)	θ	$\frac{Pr}{\Delta\tau}$	$-\frac{\theta^n}{\Delta\tau/Pr} + Pr[U\frac{\partial\theta}{\partial X} + V\frac{\partial\theta}{\partial Y}]^n - (\frac{\partial^2\theta}{\partial Z^2})^n$
Vorticity transport	ω	$\frac{1}{\Delta\tau}$	$-\frac{\omega^n}{\Delta\tau} + [U\frac{\partial\omega}{\partial X} + V\frac{\partial\omega}{\partial Y}]^n - Gr(\frac{\partial\theta}{\partial Y})^n - (\frac{\partial^2\omega}{\partial Z^2})^n$
Stream function	ψ	$\frac{1}{\Delta\tau}$	$-(\frac{\psi^n}{\Delta\tau} + \omega^n)$

This is the Helmholtz equation of the form

$$\phi_{xx} + \phi_{yy} - \lambda_\phi^2 \phi = f_\phi \tag{3.64}$$

where $\lambda_\phi^2 = 1/(\Gamma\Delta\tau)$ is a parameter that can take different positive values and f_ϕ is known forcing function that forms the right side of equation (3.64). Equation (3.54) can be discretized in the same way, treating the diffusion term implicitly and source term explicitly, and the discretized form can be also be represented by equation (3.64). Definitions of the various terms that describe the energy, stream functon, and vorticity equations are summarized in Table 3.4.

The central differencing of the diffusion term $\frac{\partial^2\phi}{\partial Z^2}$ yields

$$\frac{\partial^2\phi}{\partial Z^2} = \frac{\phi(k+1) - 2\phi(k) + \phi(k-1)}{\Delta Z^2} \tag{3.65}$$

and the first order derivative in source term of equation (3.54) can be differentiated using forward difference to obtain the following approximation:

$$\frac{\partial\theta}{\partial Z} = \frac{\phi(k+1) - \phi(k)}{\Delta Z} \tag{3.66}$$

Numerical solutions to the foregoing governing differential equations for the present problem are obtained by spectral element method. The spectral element discretization scheme used in this problem is presented in chapter 2, and the solution methodology employed here is basically the same as for rectangular enclosure problem with one extra step of marching in z direction after having obtained the steady state solution for previous z-plane.

Chapter 4

Results and Discussion

The computations have been accomplished for buoyancy driven flows and heat transfer in rectangular enclosures and in vertical fin arrays. Results, so obtained, have been compared with the finite-difference and finite-element solutions to assess the accuracy of the spectral element method.

The numerical work has been performed on the **HP 9000/735** series computer. The system has a RAM of 144 MB and 40 Mflops (scalar) peak performance.

4.1 Unsteady Natural Convection in a Square Cavity

Calculations have been performed considering air as the working fluid (Pr=0.71) for aspect ratio Ar=1.0 and $10^2 \leq Ra \leq 10^4$. The flow and temperature fields inside the cavity are illustrated by means of contour plots of streamlines, isotherms and vorticity, respectively, as shown in Figure 4.1 to 4.9. The results shown in these figures are obtained for dimensionless left side wall temperature equal to 1.0 and that of right side wall temperature equal to 0.0. The top and bottom walls are held insulated. The initial temperature, vorticity and stream function fields are chosen to be zero at time $\tau = 0$. Results are obtained using 12×12 Gauss-Lobatto points and one element in each direction. Similarly 6×6 and 4×4 Gauss-Lobatto points for each elements are used while the number of elements in each direction are 2 and 3 respectively. It was observed that a system of one element in each direction with 12×12 Gauss-Lobatto points is a good choice. The agreement between the present

Table 4.1: Average Nusselt number along the heated wall for air as working fluid (Pr = 0.71) Ar = 1.0.

Ra	Present study	Philips [15]
10^3	1.16438	1.118
10^4	2.24574	2.250

Table 4.2: Average Nusselt number along the heated wall for Pr = 1.0, Ar = 1.0 .

Ra	Present study	Shiralkar and Tien [14]
10^3	1.068	1.131
10^4	2.2774	2.277

spectral element solution and the finite difference solutions by Philips [15], Kublbeck et al. [16] and finite element solution by Ramaswamy [17] is excellent in all respects. The comparisons have been done on the basis of streamlines, isotherms and vorticity contours.

For small values of Rayleigh number ($< 10^3$), the isotherms are evenly spaced parallel lines indicating that the heat transfer is dominated by conduction and the convection effects are less (see Figure 4.1). For higher Rayleigh numbers ($\geq 10^3$), convection effect starts dominating as it is evident from distorted isotherm patterns shown in Figure 4.4 and 4.7. Isotherms for higher Rayleigh numbers result in high temperature gradients near the wall.

Figures 4.2, 4.3, 4.5, 4.6, 4.8 and 4.9 show streamlines and constant vorticity contours in the cavity for three different Rayleigh numbers.

The local Nusselt number distribution along the heated wall of the cavity is reported in Figure 4.10 for Ra = 10^3 and 10^4. The Nusselt number gradually decreases along the vertical wall. It is interesting to note from this figure that the maximum value of the Nusselt number occurs at a location slightly above the lower wall.

The average Nusselt number along the heated wall is documented in Table 4.1. Results are compared with those of Philips [15]. Philips [15] had reported the results due to finite difference method using 65 × 65 grid pints. The results for the Spectral Element method using 12 × 12 Gauss-Lobatto points show a reasonably good agreement with the reported results.

Again for the purpose of comparison of our results with those of Shiralkar and Tien [14], the same problem has been solved for Pr=1.0 and for a range of Rayleigh

number. The Nusselt number values due to present computation are reported in Table 4.2. Table 4.2 also shows the corresponding Nusselt numbers predicted by Shiralkar and Tien. The results of present study agree well with the results of Shiralkar and Tien.

It has been observed that when Rayleigh number increases and becomes equal or greater than 10^5, the solution starts oscillating and the steady state values are not obtainable. It is conjectured that the flow displays an oscillating behaviour which corresponds to a typical time-periodic motion.

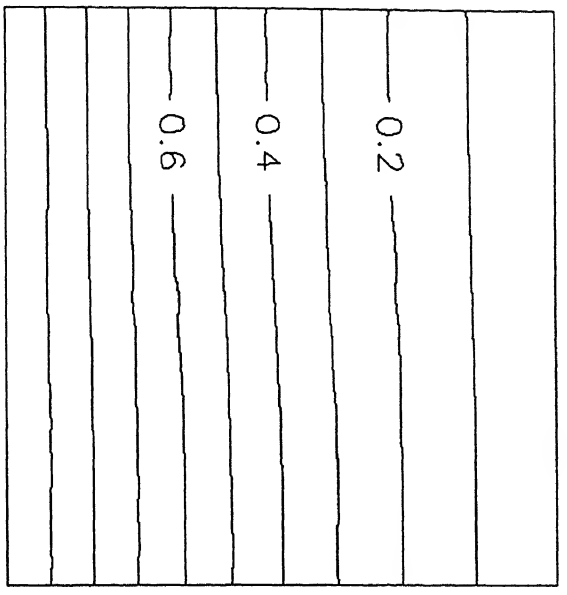

Figure 4.1: Isotherms for square cavity : Ra=10^2 and Pr=0.71

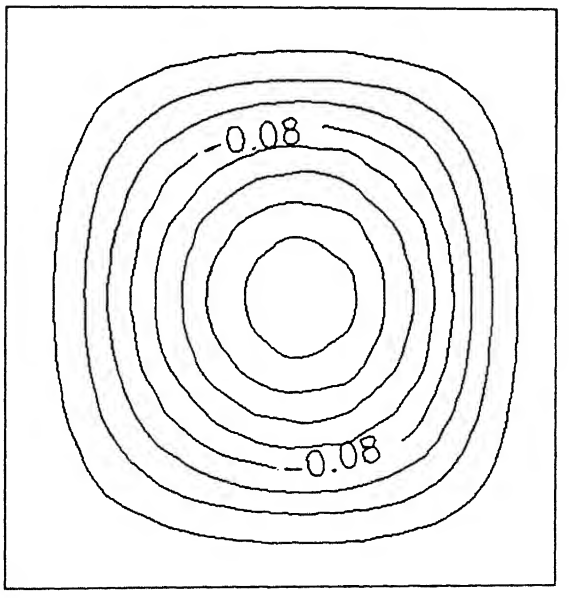

Figure 4.2: Streamlines for square cavity : Ra=10^2 and Pr=0.71

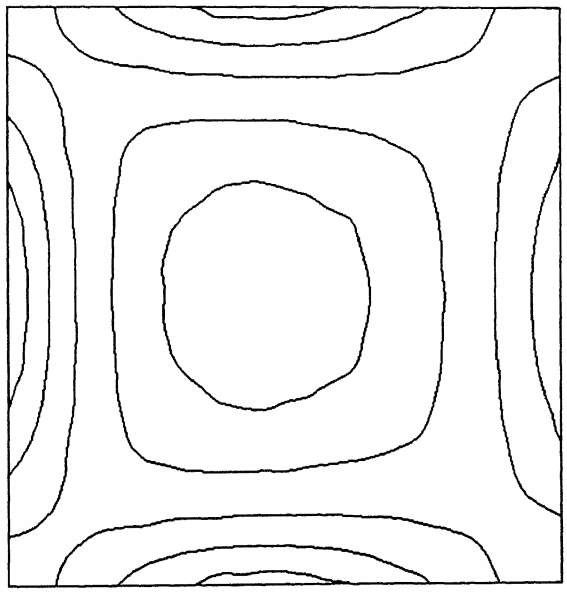

Figure 4.3: Vorticity contours for square cavity : Ra=10^2 and Pr=0.71

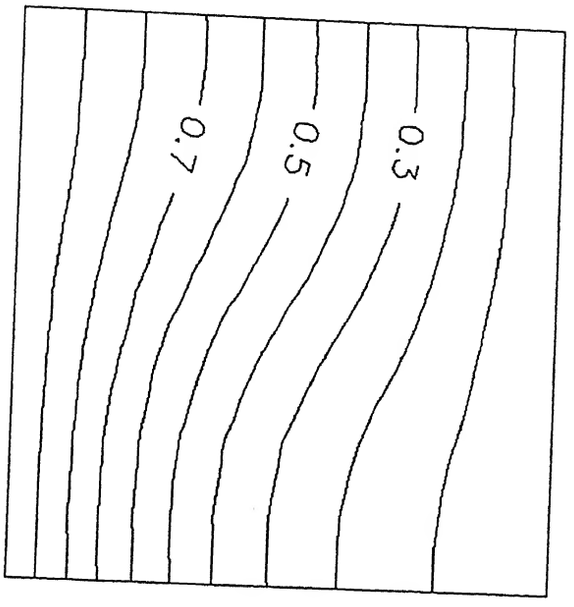

Figure 4.4: Isotherms for square cavity : Ra=10^3 and Pr=0.71

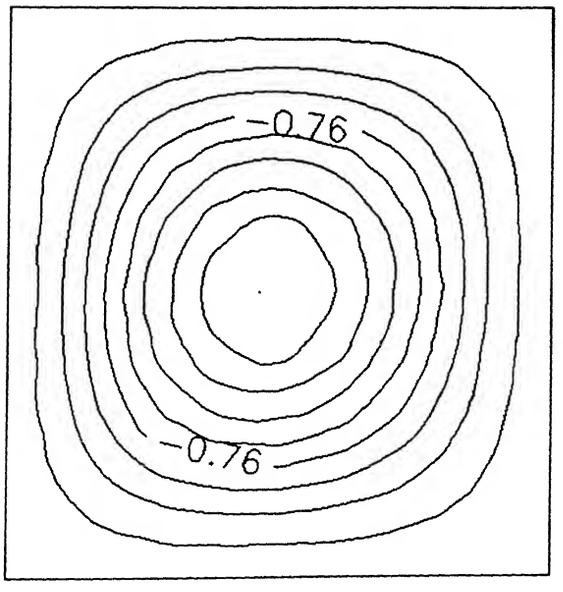

Figure 4.5: Streamlines for square cavity : Ra=10^3 and Pr=0.71

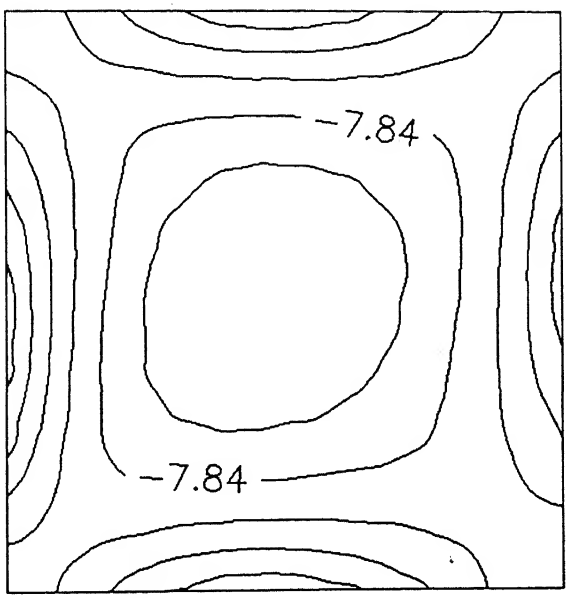

Figure 4.6: Vorticity contours for square cavity : Ra=10^3 and Pr=0.71

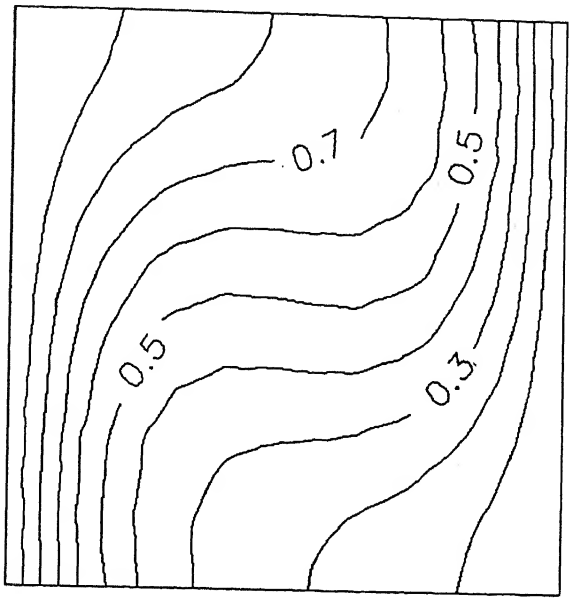

Figure 4.7: Isotherms for square cavity : Ra=10^4 and Pr=0.71

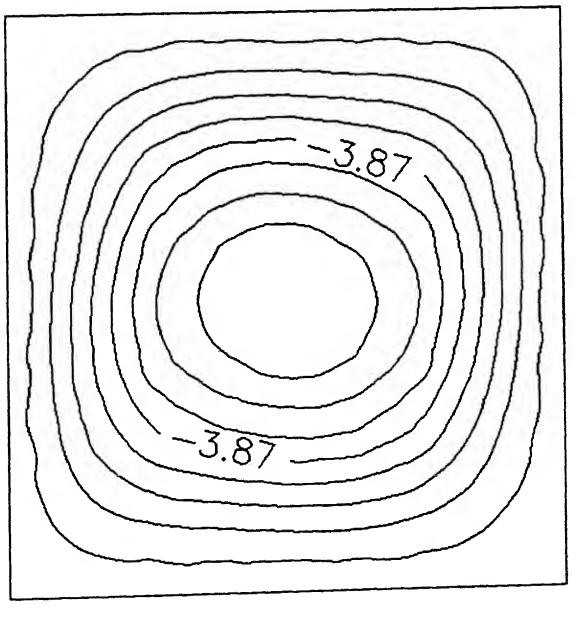

Figure 4.8: Streamlines for square cavity : Ra=10^4 and Pr=0.71

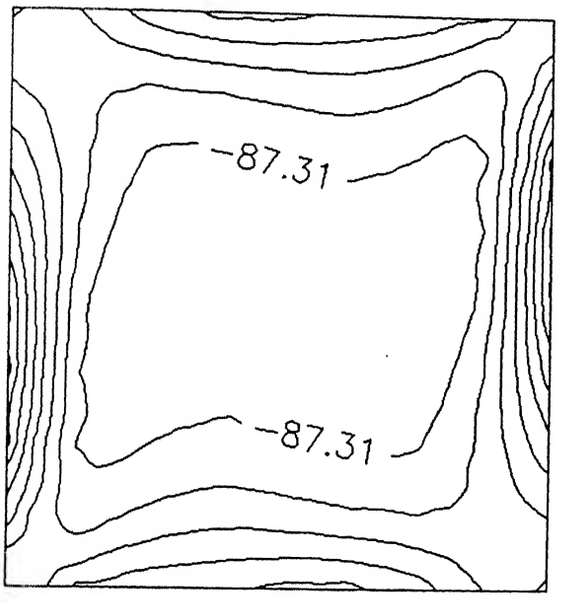

Figure 4.9: Vorticity contours for square cavity : Ra=10^4 and Pr=0.71

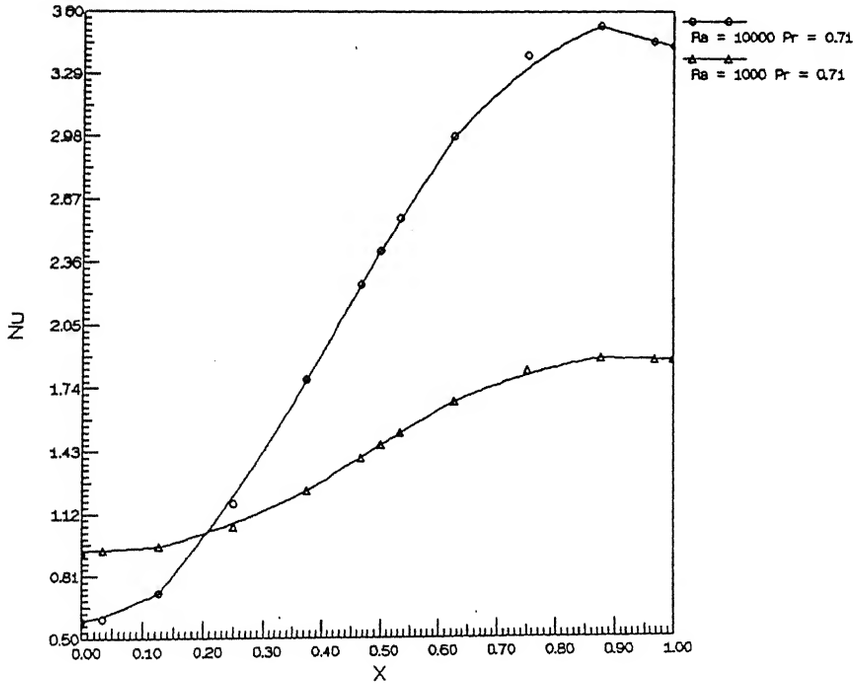

Figure 4.10: Local Nusselt number variation on the heated wall for square cavity

4.1.1 The Effect of Aspect Ratio

To study the effect of aspect ratio on the temperature and flow field, a problem of natural convection in rectangular enclosure is solved. The temperature boundary conditions taken on the left and right side walls are 0.5 and -0.5 respectively with adiabatic top and bottom walls. Other boundary conditions remaining the same as explained earlier. The initial conditions for θ, ω, and ψ at $\tau = 0$ are zero. The calculations have been performed for $Ra = 1.446 \times 10^4$ and Pr = 0.733. Figure 4.11 shows the isotherms, streamlines and vorticity contours for a rectangular enclosure of aspect ratio 3. The present results agree qualitatively with those of Ramaswamy [17].

Finally, Figures 4.12 and 4.13 show similar results for a rectangular enclosure of aspect ratio 1.83, with the temperature boundary conditions -0.5 and 0.5 respectively on left and right side walls. The results shown in these figures are obtained for a Rayleigh number of 10^4 and Pr = 1.0. Results for the same problem of aspect ratio of 1.83 but with linear temperature distribution on the horizontal walls are reported in Figures 4.14 and 4.15 . The top boundary temperature distribution is governed by the linear relation $\theta(0, Y) = -0.5 + Y$ while the bottom boundary of the enclosure is maintained at $\theta(1, Y) = -0.4$. Szekely and Todd [19] have reported the experimental and finite difference solution results for this problem for Ra = 8200 and Pr = 2450.

It was observed that for larger aspect ratios the numerical solutions converged slower.

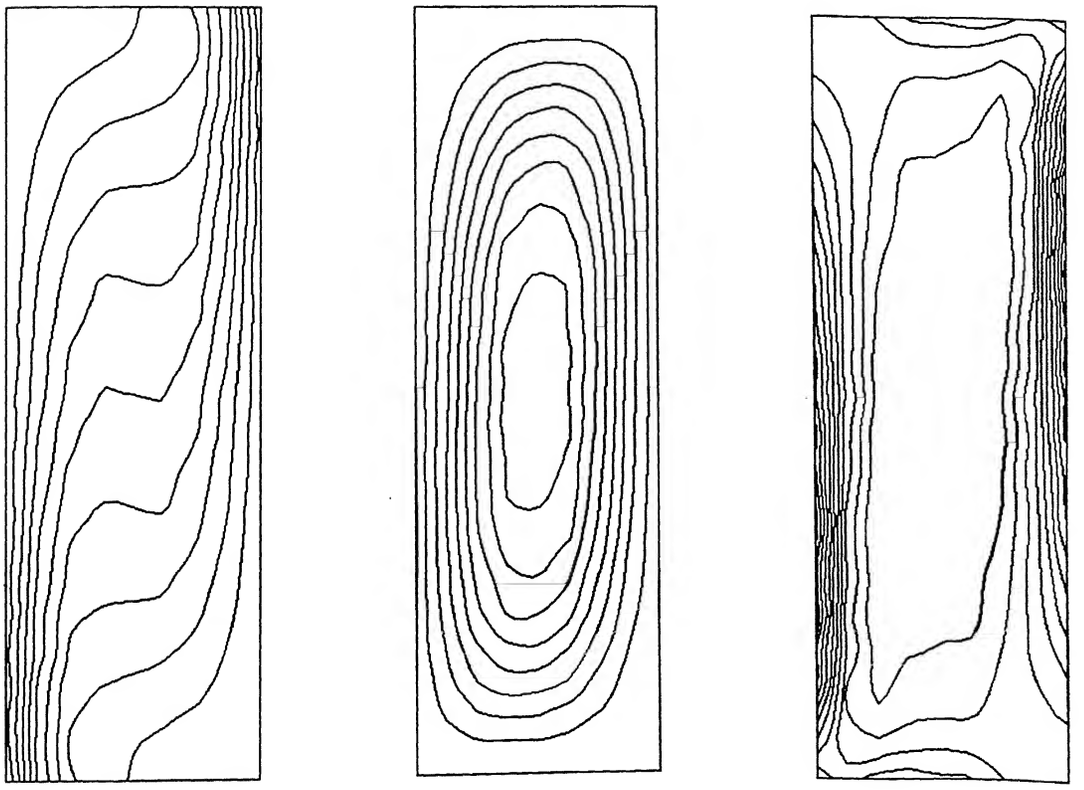

(a) (b) (c)

Figure 4.11: (a) Isotherms, (b) streamlines and (c) vorticity contours for Ra=1.446 $\times$ 10^4, Pr=0.733 and Ar=3.0

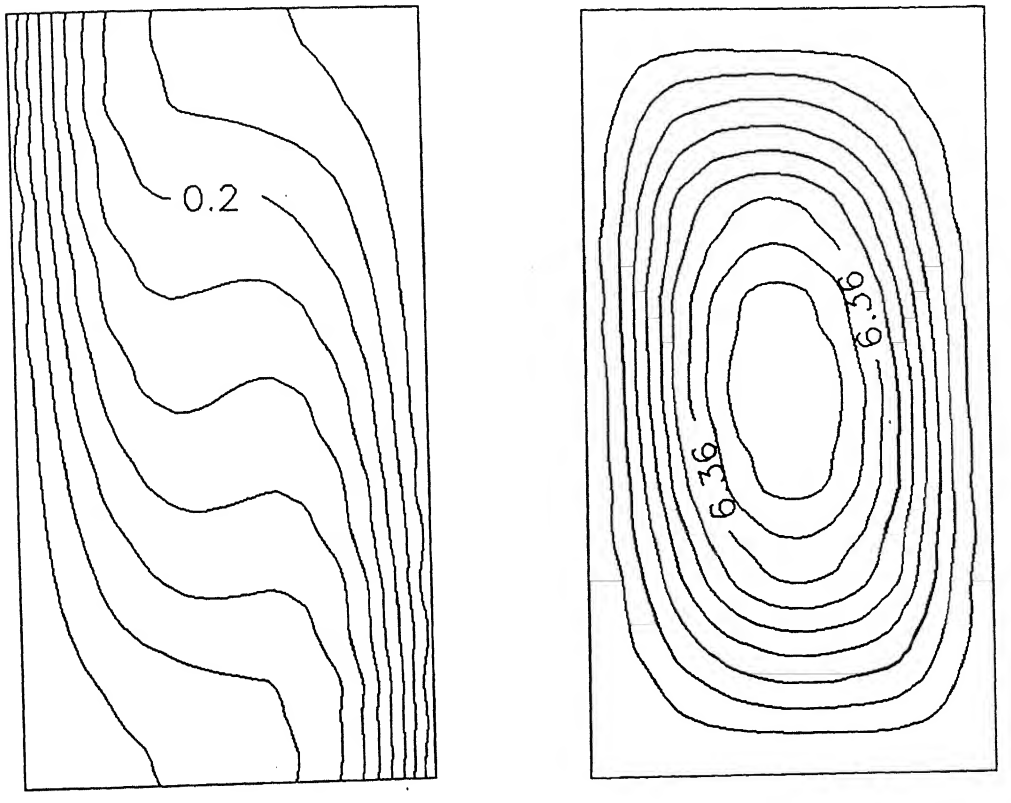

(a) (b)

Figure 4.12: (a) Isotherms and (b) streamlines for rectangular enclosure at Ra=10^4, Pr=1 and Ar=1.83

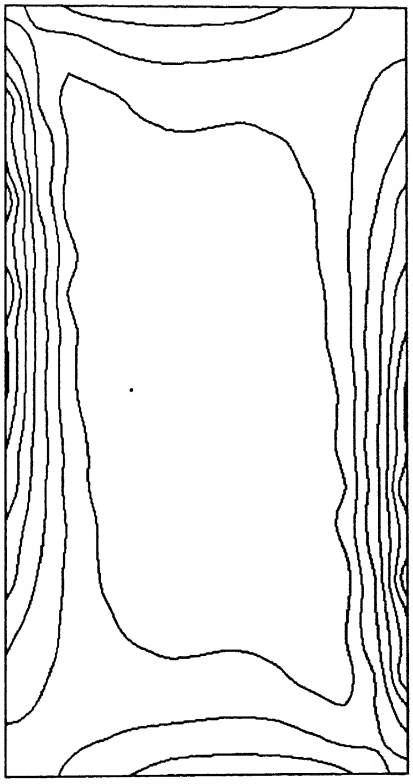

Figure 4.13: Vorticity contours for rectangular enclosure at Ra=10^4, Pr=1 and Ar=1.83

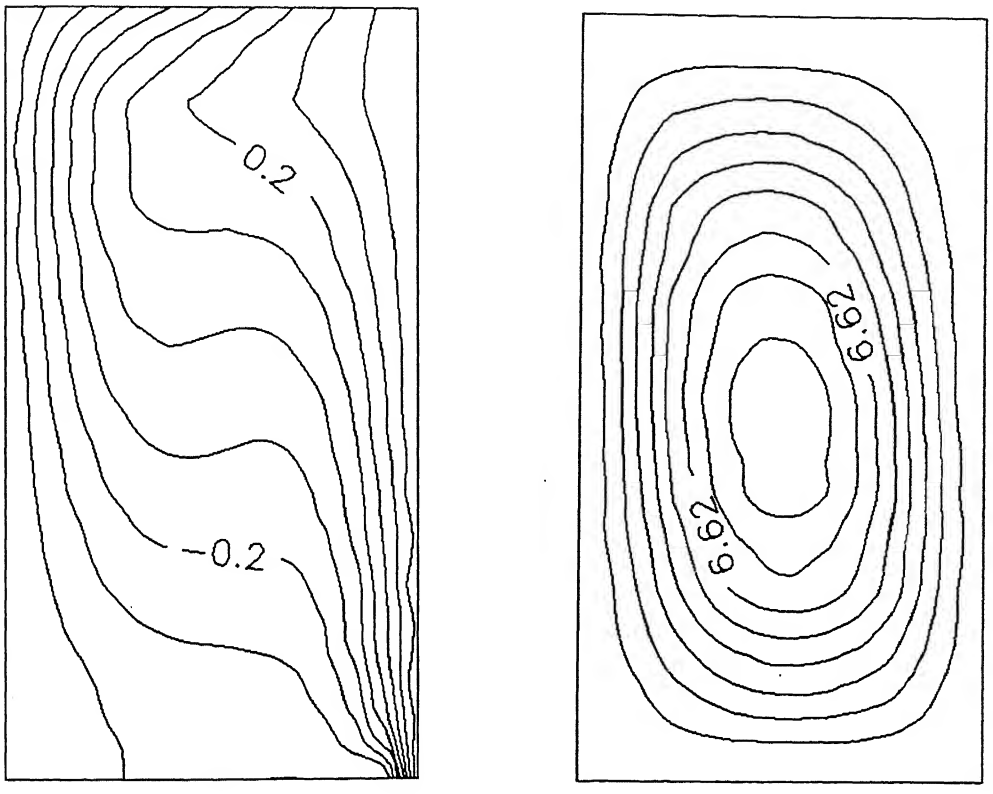

(a) (b)

Figure 4.14: (a) Isotherms and (b) streamlines for rectangular enclosure at Ra=10^4, Pr=1 and Ar=1.83

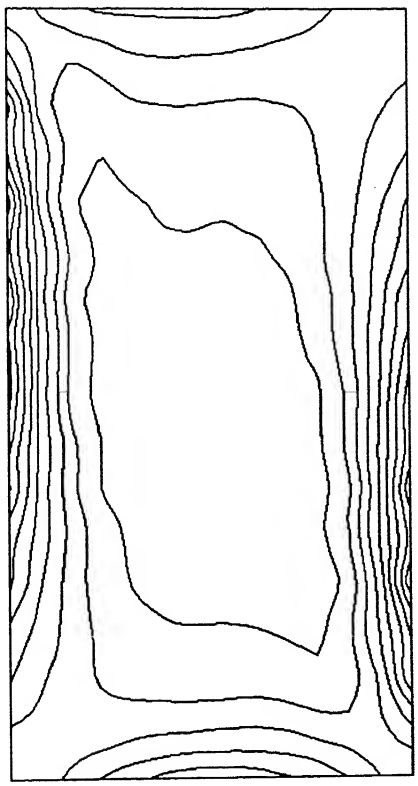

Figure 4.15: Vorticity contours for rectangular enclosure at Ra=10^4, Pr=1 and Ar=1.83

4.2 Natural Convection Heat Transfer in a Vertical Rectangular Enclosure with Discrete Heating

A computational study of natural convection in an enclosure as applied to applications in cooling of electronic components is reported.

The computations are first carried out for aspect ratio (Ar = 6), $Ra^{\star} = 10^3$ and Pr = 0.71. The relative heater size, l/H, and the location, s/H, on the vertical wall are fixed at 1/30 and 13/75, respectively. The qualitative behaviour of streamlines and isotherms inside the discretely heated enclosure is found to have good agreement with the results of Ho and Chang [20]. Ho and Chang used a mesh system consisting of a uniform grid of 151 in the x direction and a non uniform grid of 51 in y direction to generate the numerical simulations for the present problem. The present analysis employs 9 elements in x-direction and 1 element in y-direction. In each element 7 Gauss-Lobatto points have been used in x- and y-directions respectively.

At $Ra^{\star} = 10^3$, heat of the discrete heaters is essentially dissipated via a conduction-dominated mechanism as indicated by the isotherm pattern around the discrete heaters shown in Figure 4.16. With increase of the aspect ratio of the enclosure, the buoyant convection flow is increasingly strengthened, exhibiting a transformation from a primarily clockwise unicellular flow into a structure characterized by regularly spaced multicellular flow in the core region for $Ar \geq 6$, as depictedby the streamlines in Figure 4.17. These split core vortices are essentially in parallel with the location of the heaters on the vertical wall.

Figure 4.18 shows the predicted isotherms and streamlines pattern for $Ra^{\star} = 4.0 \times 10^4$ and Ar =10. It is noteworthy that the present predictions agree qualitatively well with the experimental and numerical predictions of Ho and Chang [20].

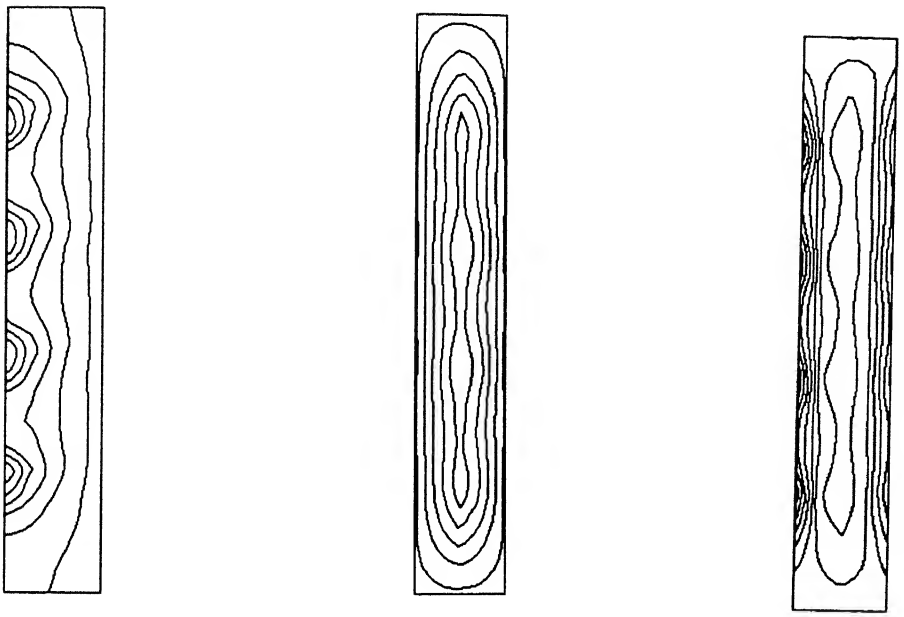

Figure 4.16: (a) Isotherms, (b) streamlines and (c) vorticity contours for discretely heated rectangular enclosure at $Ra^{\star} = 10^3$, Pr=0.71 and Ar=6.

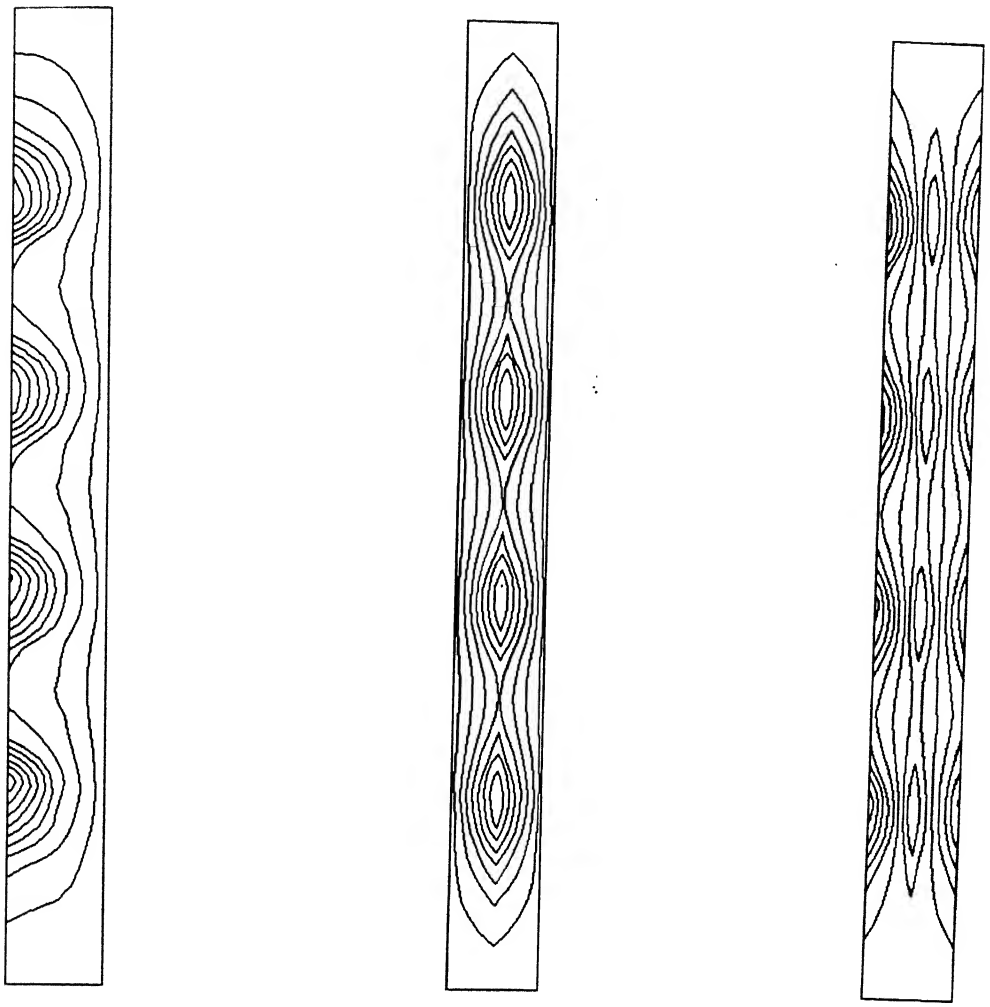

Figure 4.17: (a) Isotherms, (b) streamlines and (c) vorticity contours for discretely heated rectangular enclosure at $Ra^{\star} = 10^3$, Pr=0.71 and Ar=10.

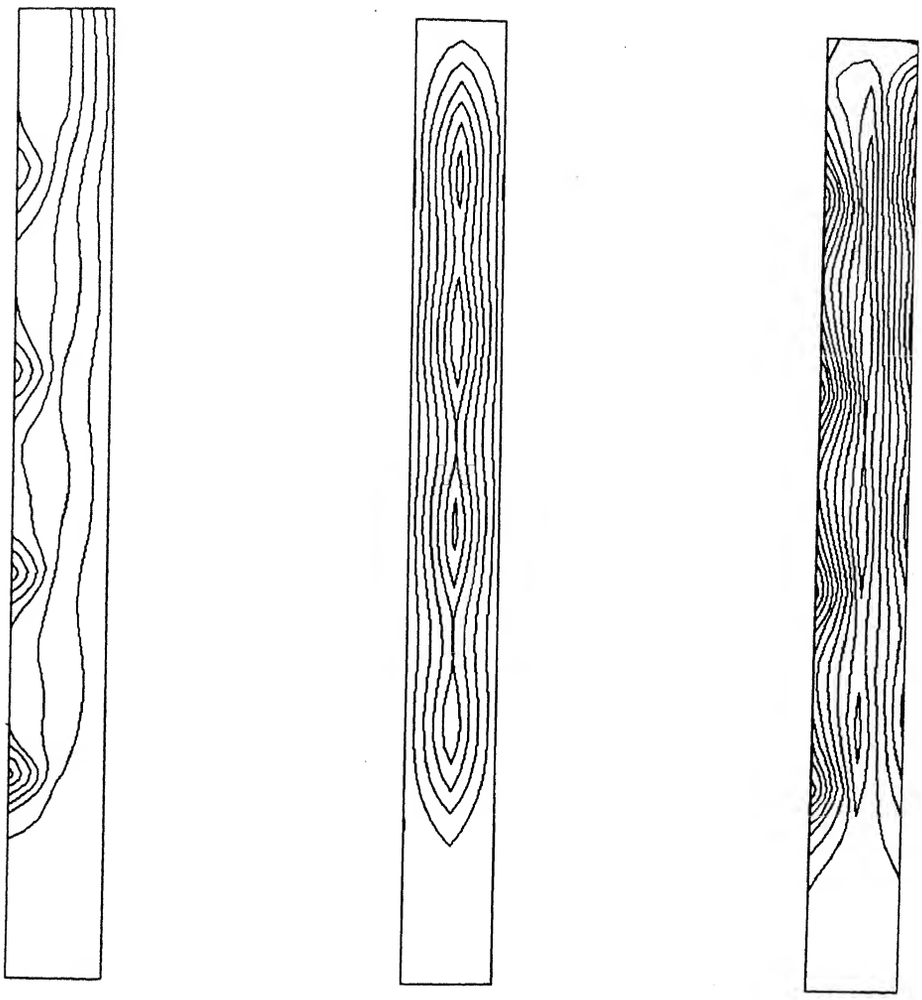

Figure 4.18: (a) Isotherms, (b) streamlines and (c) vorticity contours for discretely heated rectangular enclosure at $Ra^{\star} = 4.0 \times 10^4$, Pr=0.71 and Ar=10.

4.3 Flow Analysis in Vertical Fin Arrays

The computations have been carried out assuming air (Pr=0.71) as the working fluid. The results are reported for Rayleigh numbers of 10^4 and 10^5.

The temperature distribution on the fin surface is obtained by solving the transient heat conduction equation. Subsequently the advection diffusion equation is dealt with. The fins are assumed to have a high thermal conductivity. The following property values have been used:

$$\alpha_s = 8.418 \times 10^{-5}\ m^2/s, \qquad \rho_s = 2707\ \text{Kg}/m^3, \qquad k_s = 204\ \text{W/m}^\circ C,$$
$$c_{ps} = 0.896\ \text{KJ/Kg}^\circ C$$

As mentioned earlier, air has been assumed as the working fluid and the following property values have been used for air wherever needed

$$\alpha_a = 0.2216 \times 10^{-4}\ m^2/s, \qquad \nu_a = 15.69 \times 10^{-6}\ m^2/s, \qquad k_a = 0.02624\ \text{W/m}\ ^\circ C,$$

The fins are jutting out from a vertical base. As they have negligible thickness; the H/δ is as high as 10 in the present computations. The Rayleigh numbers used in the present problem are 10^4 and 10^5. The Spectral Element technique has been deployed to solve the governing equations for vorticity transport. Fig.3.4 shows 4×4 elements on the x-y plane. The fin is an element which has a count as the third element in x-direction and the first element in y-direction. The height and the length of the fin are taken as 1.0 (nondimensional).

Figures 4.19(a) to 4.25(a) show the isotherms on different x-y planes at an interval of $\Delta Z = 0.16$ for a Rayleigh number (Ra) of 10^4 and Prandtl number (Pr) of 0.71. The first x-y plane [Fig. 4.19(a)] shows the isotherms on the fin element and the immediate neighbourhood. Figures 4.20(a) to 4.25(a) depict the temperature distribution of the flowing fluid at different vertical planes. The temperature distribution at the symmetric mid-plane is shown in Fig. 4.25(a). It can be seen that the temperature is advected markedly in the x-direction.

Figures 4.26(a) to 4.32(a) show the isotherms on various x-y planes for a Rayleigh number of 10^5. The same qualitative trend of distribution of the isotherms, as it has been seen for Ra = 10^4, is observed in all the cases. However, the quantitative values of the isotherms for Ra = 10^5 are somewhat different than those for Ra = 10^4 on the same x-y planes.

Figures 4.19(b) to 4.25(b) show the streamlines on seven different x-y planes at an interval of $\Delta Z = 0.16$ for a Rayleigh number of 10^4. A buoyancy driven flow pattern

Table 4.3: Area average Nusselt number on fin surface.

Ra	10^4	10^5
Pr	0.71	0.71
$\overline{Nu}_{sa}$	8.99	9.23

is discerned through the numerical flow visualization on each x-y plane [essentially Fig. 4.20(b) to 4.25(b)] mentioned above. The streamlines are formed by the cold air entering from the bottom and front openings through multiple plumes. This flow structure basically follows a single-chimney like flow pattern. The flow structure is self-sustained since fin to air heat transfer promotes the fluid motion. Figures 4.26(b) to 4.32(b) illustrate the streamlines on all seven x-y planes, as described earlier, for a Rayleigh number of 10^5. The streamline distribution on all the planes confirms a single-chimney type flow structure through the arrays. It is evident that with increasing Rayleigh number (so to speak, with increasing temperature difference) the cold air enters from the open end at the bottom and leaves through the open end at the top.

Due to pausity of time, a detailed parametric study for various Rayleigh number and Prandtl number could not be accomplished. However, for two different Rayleigh numbers of 10^4 and 10^5 the values of area average Nusselt number are reported in Table 4.3.

For a similar geometrical configuration like the present investigation and for a Rayleigh number of 2.593×10^4, Shalaby et al. [23] obtained a value for $\overline{Nu}_{sa}$ as 9.05. This does not directly indicate the accuracy of our computation but confirms the acceptability of the predictive procedure.

The value of $\overline{Nu}_{sa}$ for a Rayleigh number of 0.71×10^5 on a vertical isothermal plate of height 10 cm losing heat by natural convection comes out be approximately 20. Thus it is seen that the values for the array are lower than for a plate alone. It will be interesting to investigate whether the $\overline{Nu}_{sa}$ value for the fin approaches the $\overline{Nu}_{sa}$ value of the plate as the spacing increases for an identical Rayleigh number.

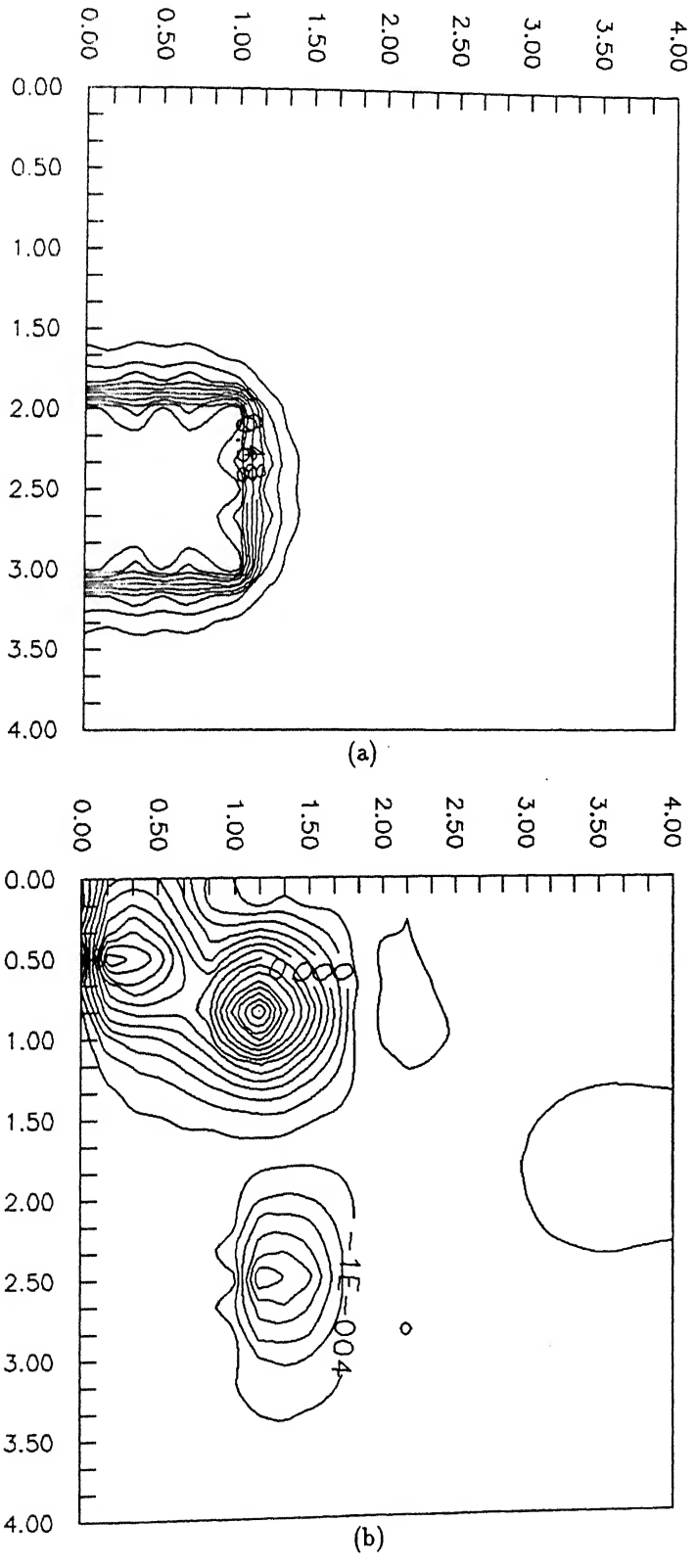

Figure 4.19: (a) Isotherms and (b) Streamlines at Plane 1 : Ra=10^4 and Pr=0.71

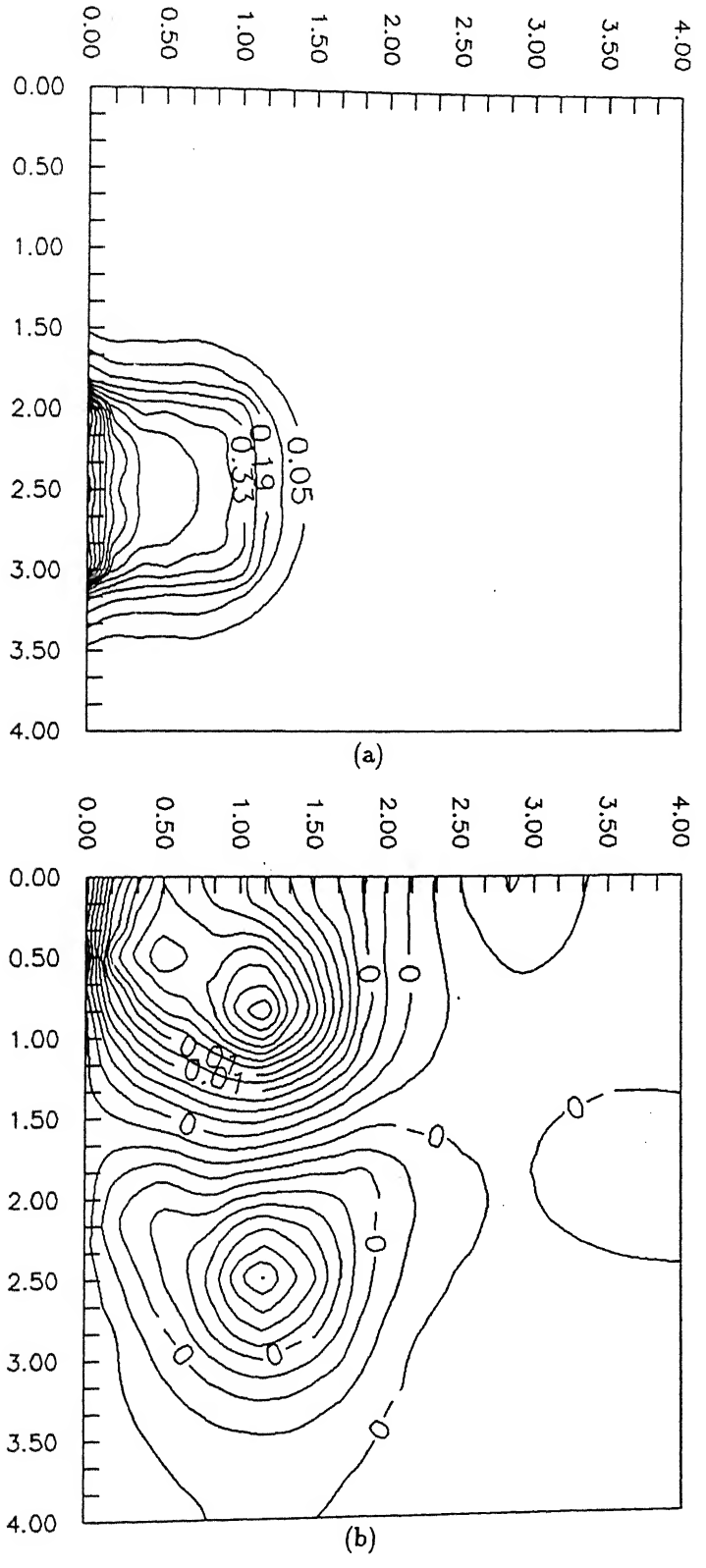

Figure 4.20: (a) Isotherms and (b) Streamlines at Plane 2 : Ra=10^4 and Pr=0.71

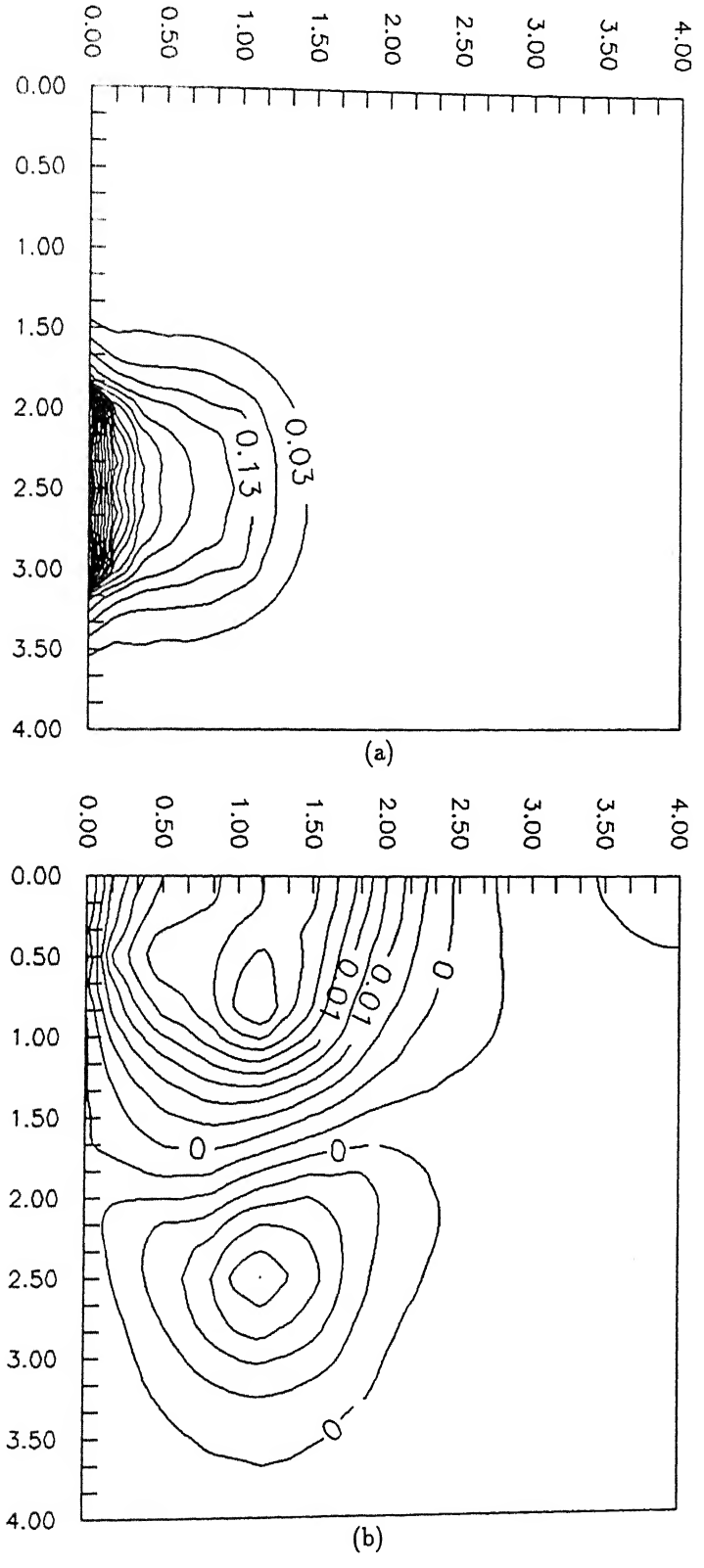

Figure 4.21: (a) Isotherms and (b) Streamlines at Plane 3 : Ra=10^4 and Pr=0.71

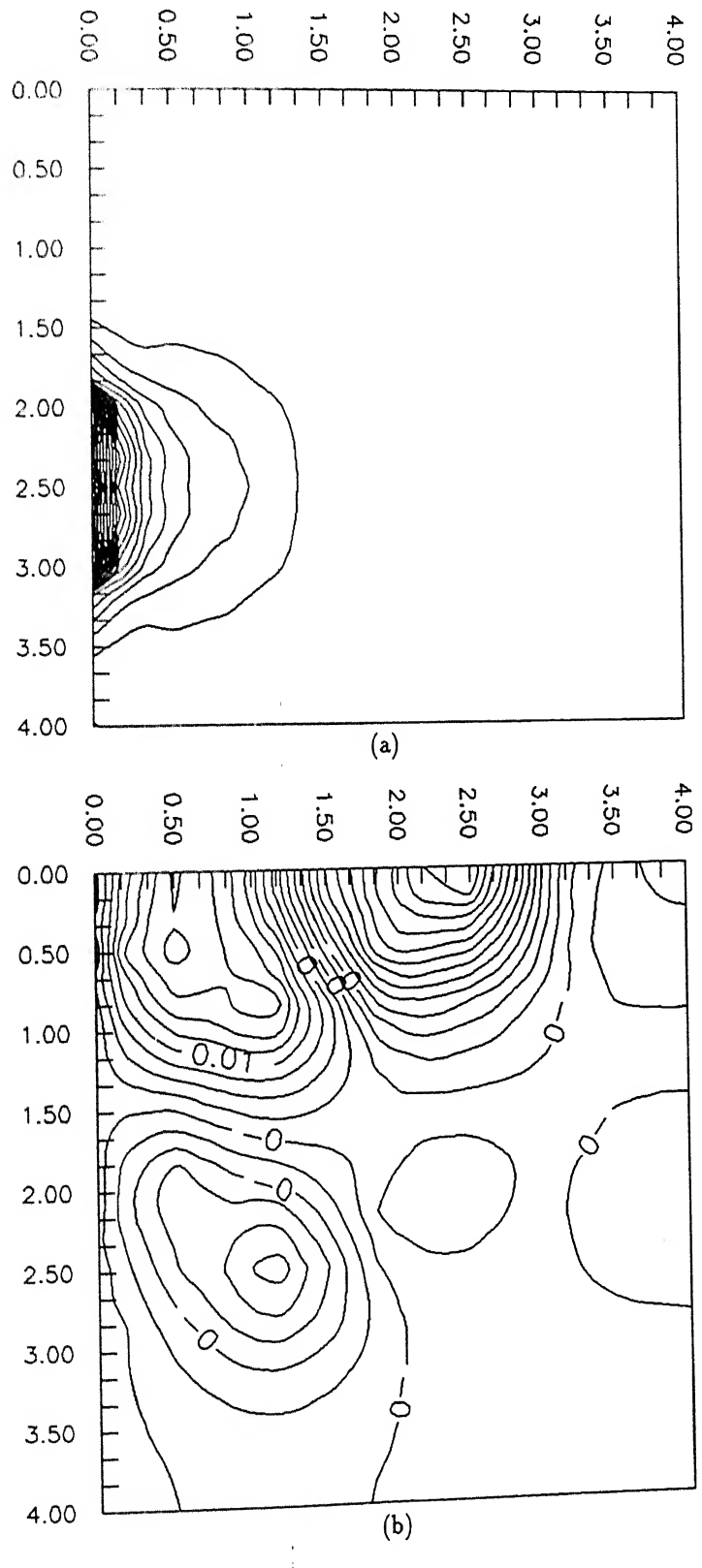

Figure 4.22: (a) Isotherms and (b) Streamlines at Plane 4 : Ra=10^4 and Pr=0.71

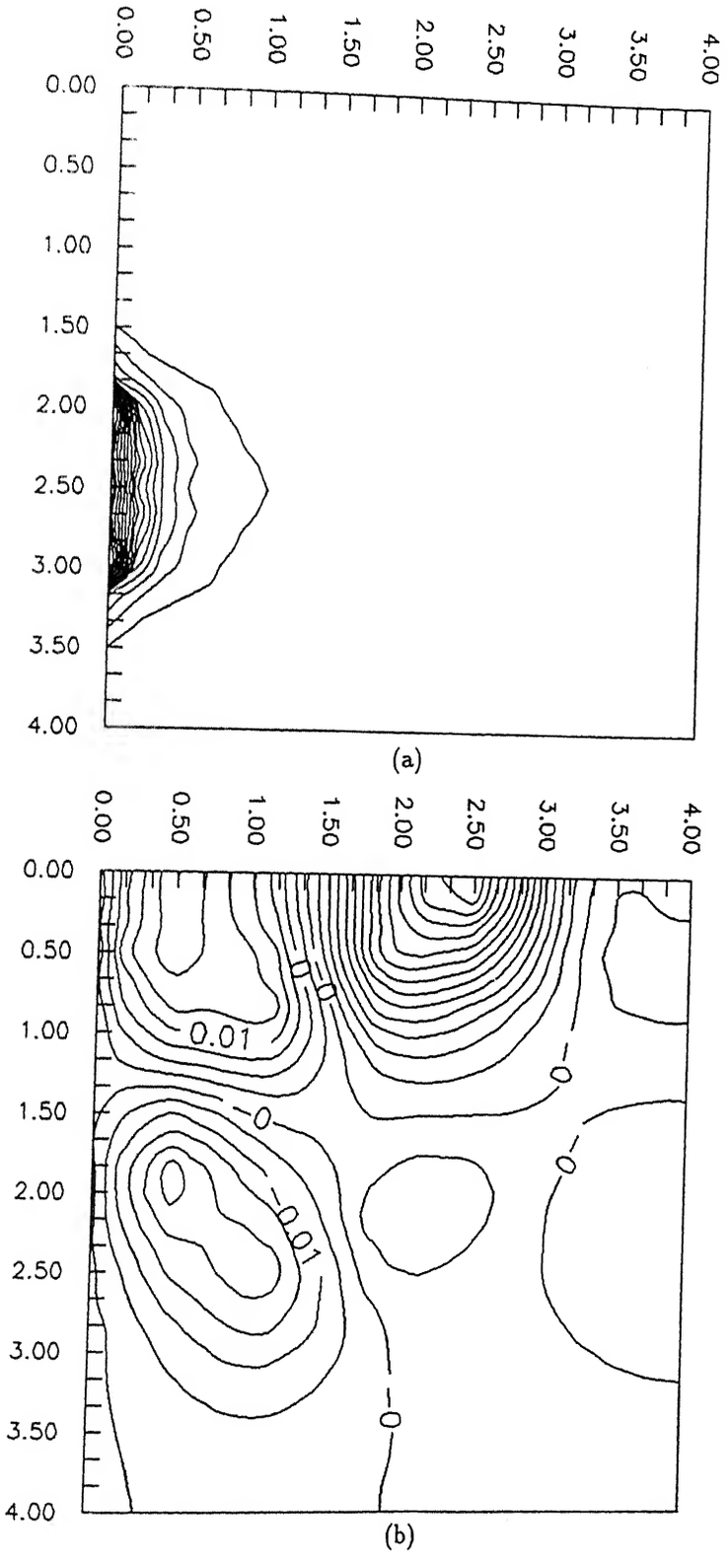

Figure 4.23: (a) Isotherms and (b) Streamlines at Plane 5 : Ra=10^4 and Pr=0.71

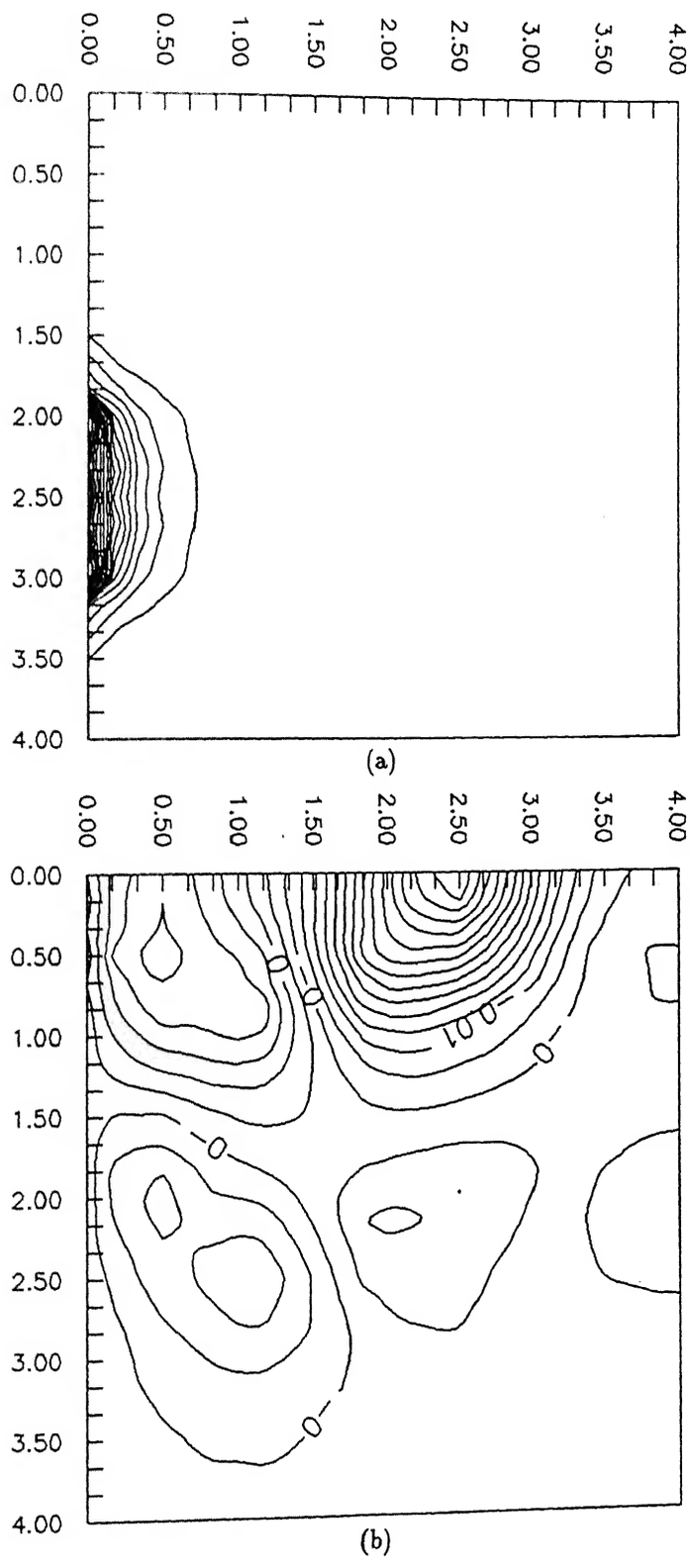

Figure 4.24: (a) Isotherms and (b) Streamlines at Plane 6 : Ra=10^4 and Pr=0.71

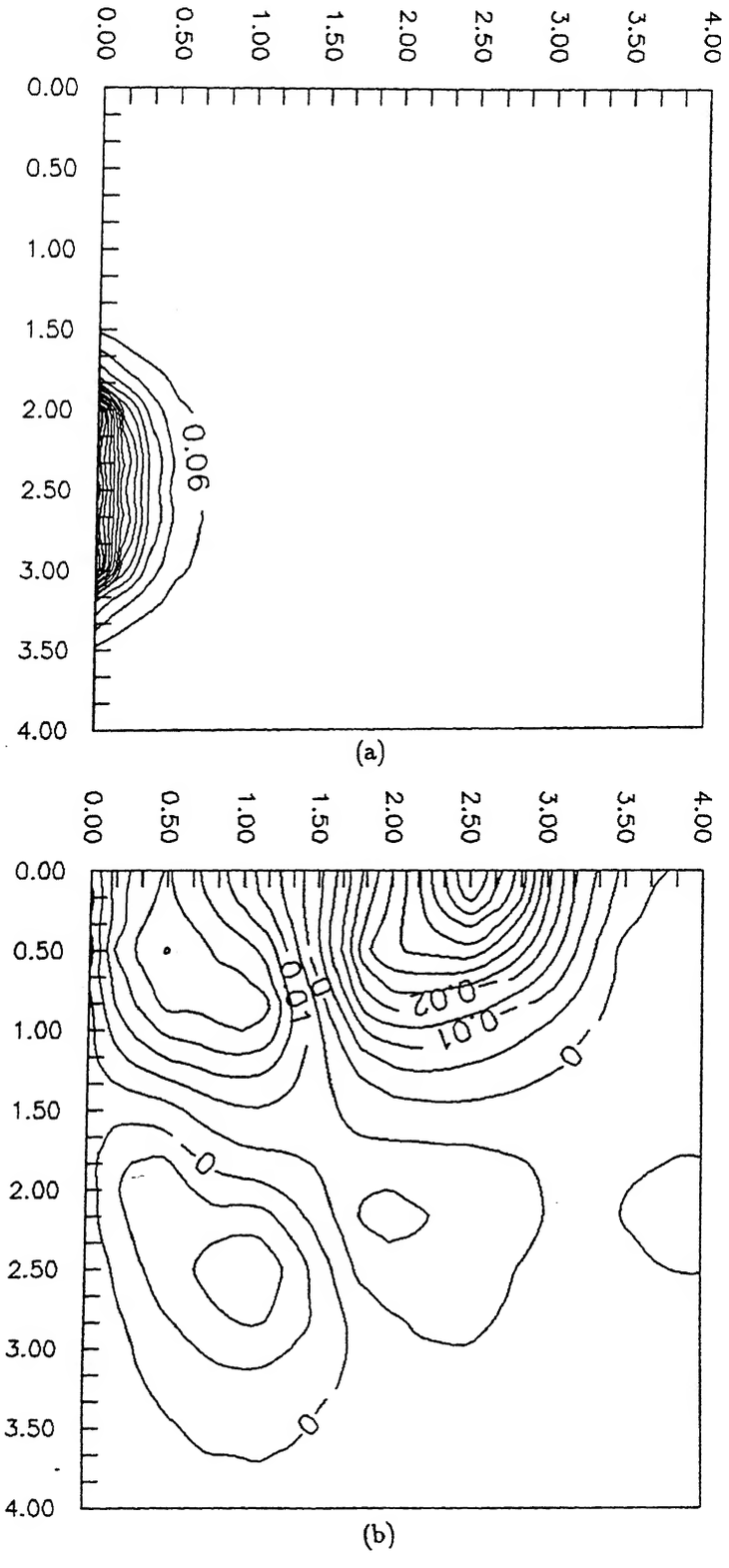

Figure 4.25: (a) Isotherms and (b) Streamlines at Plane 7 : Ra=10^4 and Pr=0.71

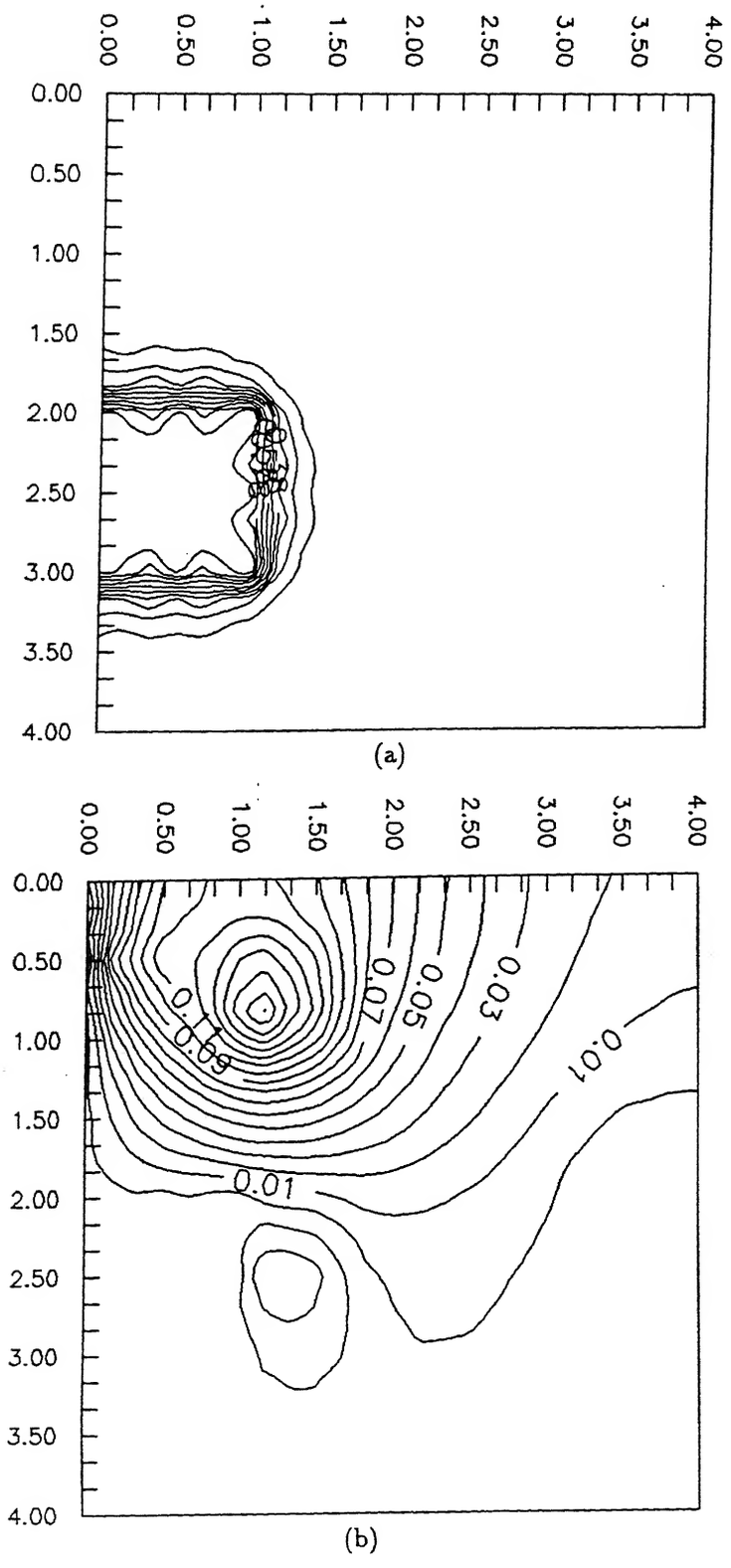

Figure 4.26: (a) Isotherms and (b) Streamlines at Plane 1 : Ra=10^5 and Pr=0.71

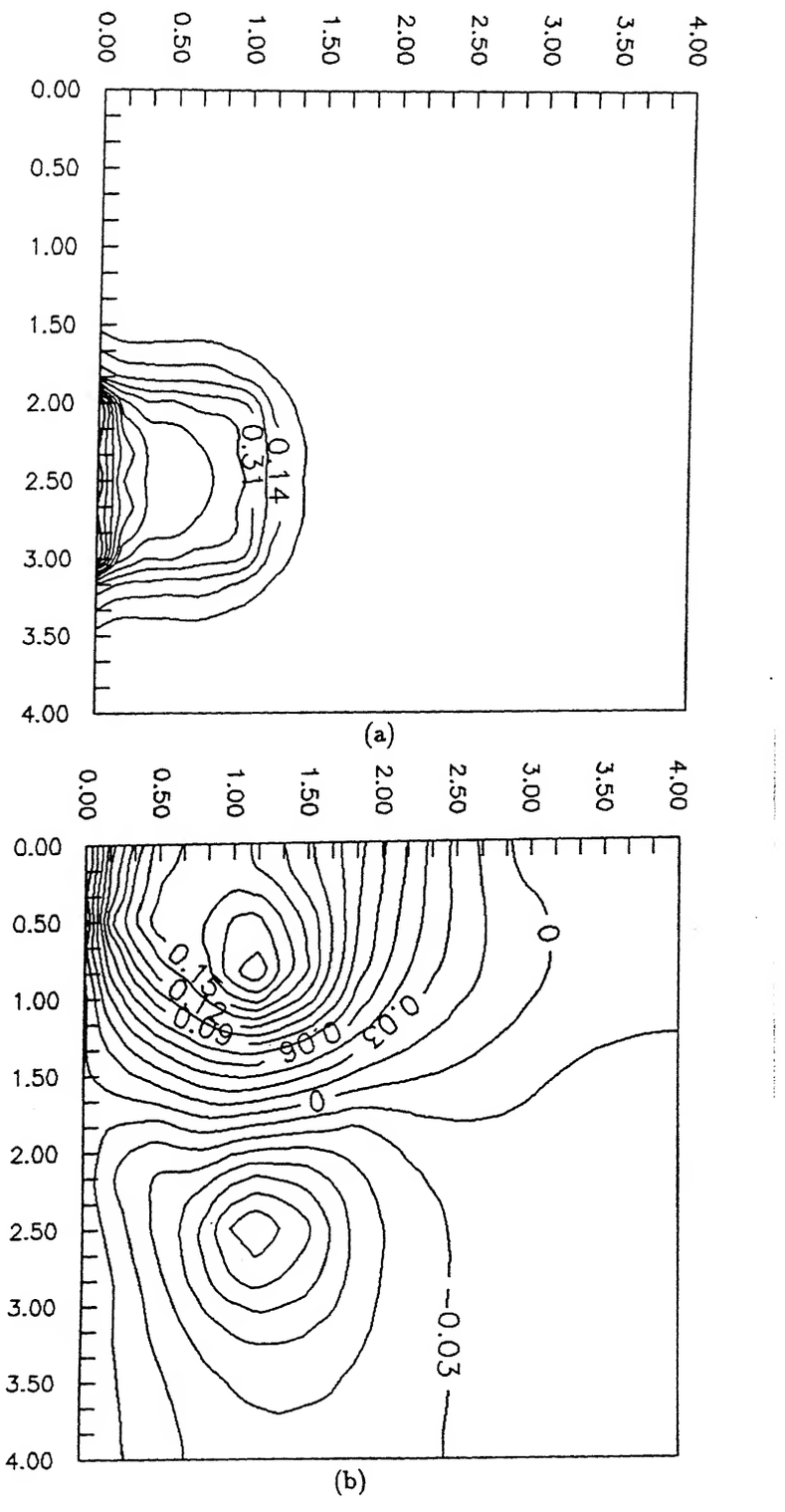

Figure 4.27: (a) Isotherms and (b) Streamlines at Plane 2 : Ra=10^5 and Pr=0.71

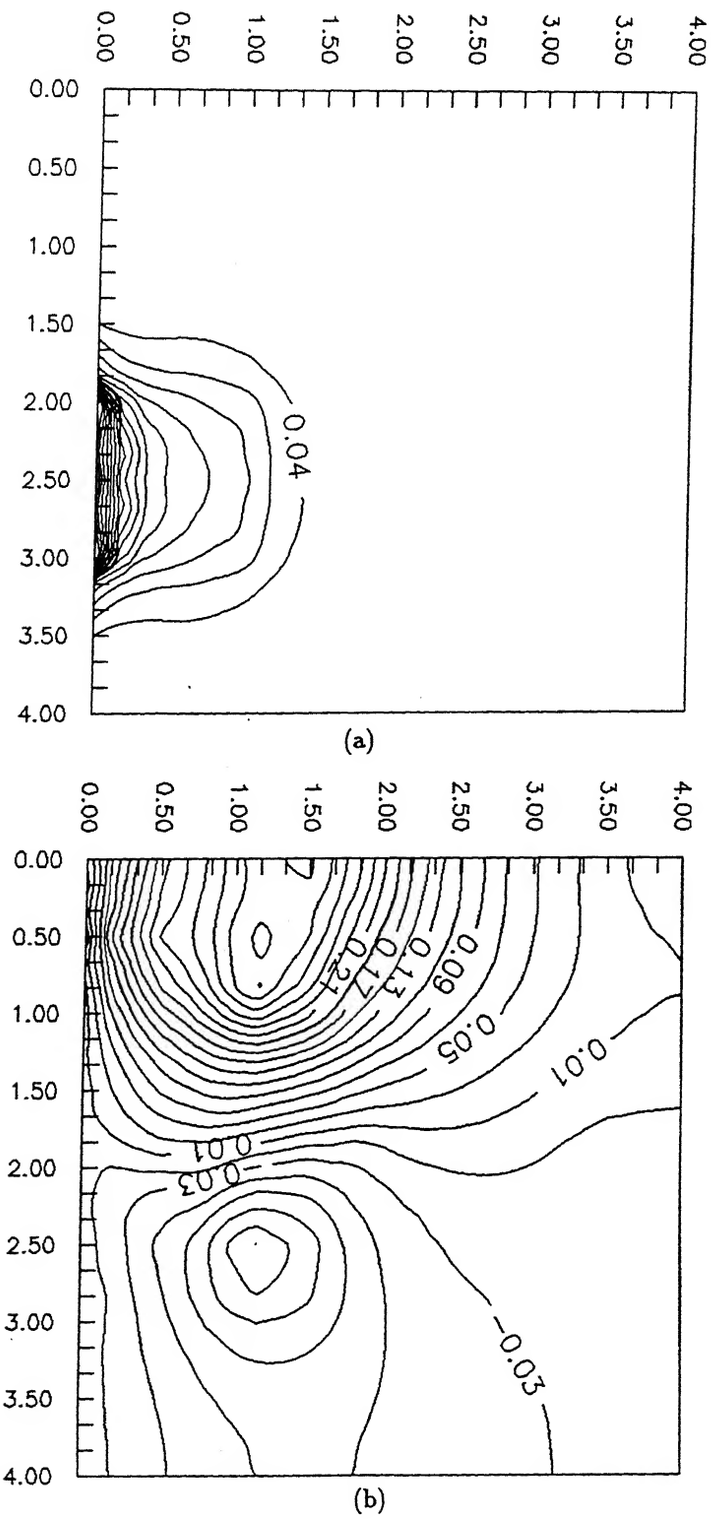

Figure 4.28: (a) Isotherms and (b) Streamlines at Plane 3 : Ra=10^5 and Pr=0.71

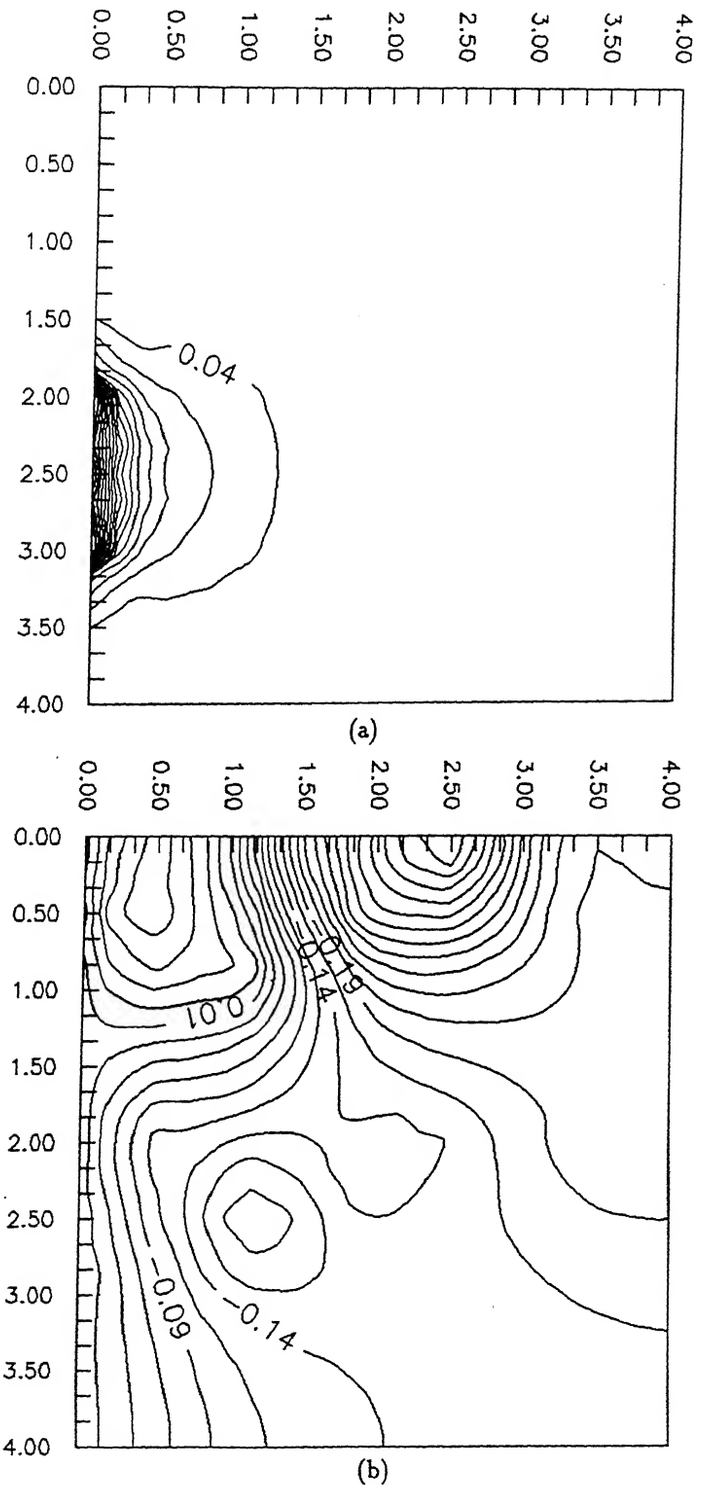

Figure 4.29: (a) Isotherms and (b)Streamlines at Plane 4 : Ra=10^5 and Pr=0.71

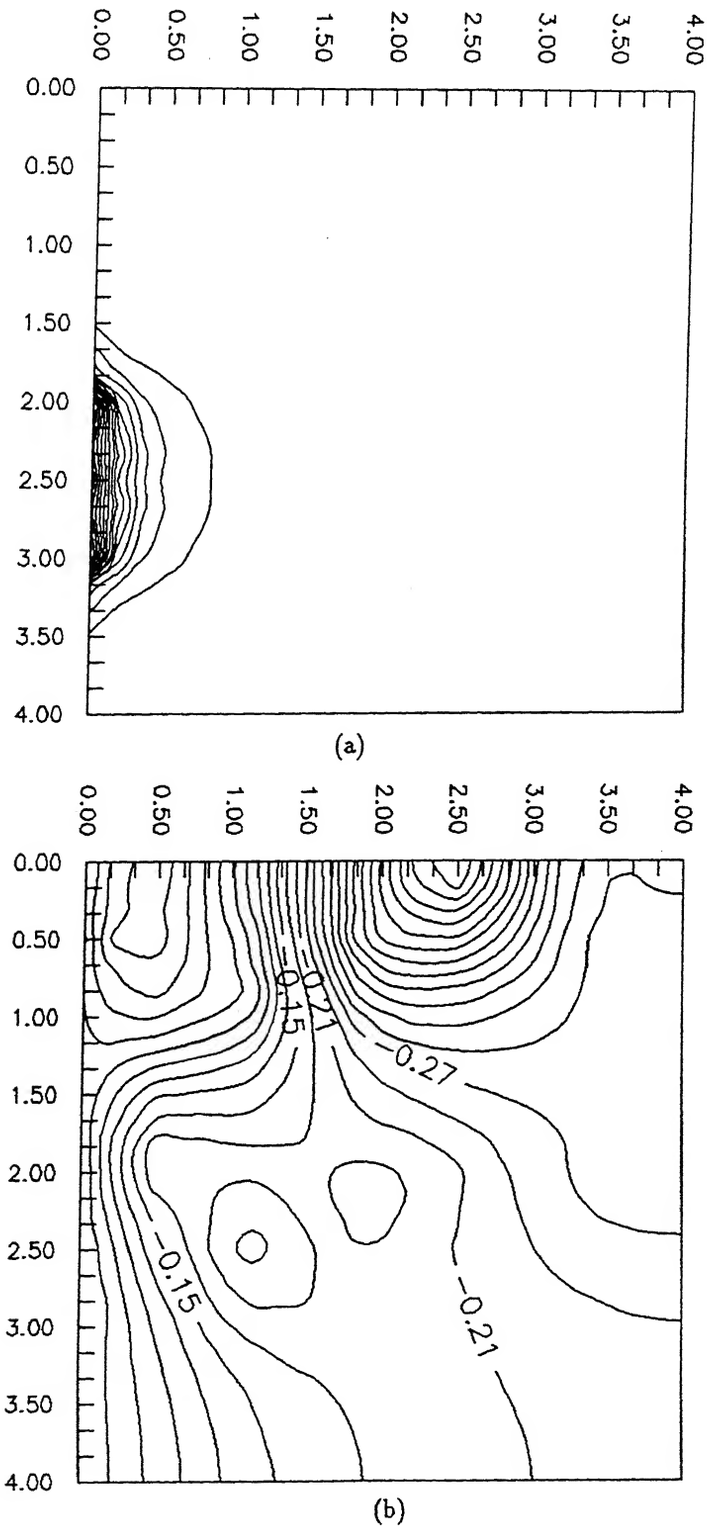

Figure 4.30: (a) Isotherms and (b) Streamlines at Plane 5 : Ra=10^5 and Pr=0.71

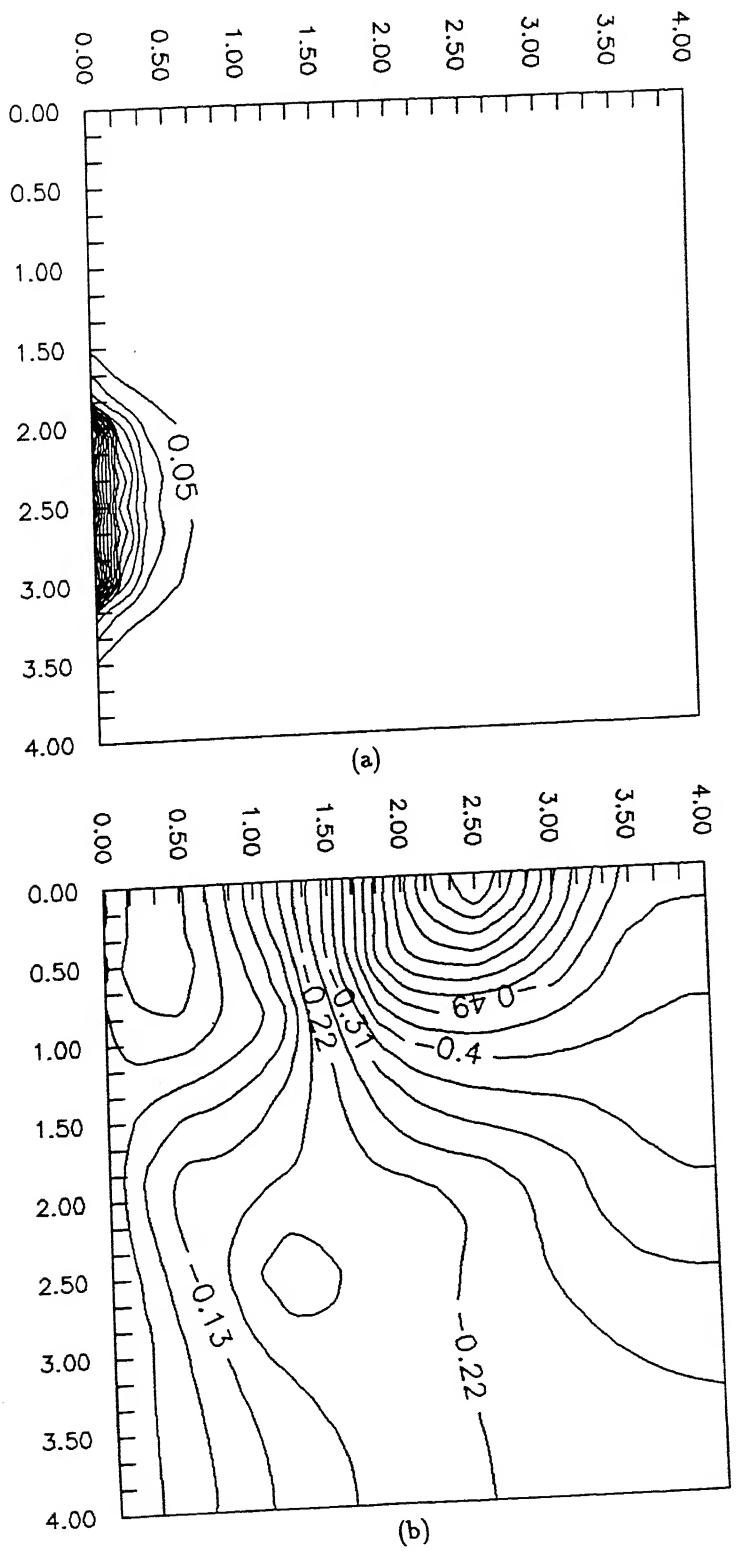

Figure 4.31: (a) Isotherms and (b) Streamlines at Plane 6 : Ra=10^5 and Pr=0.71

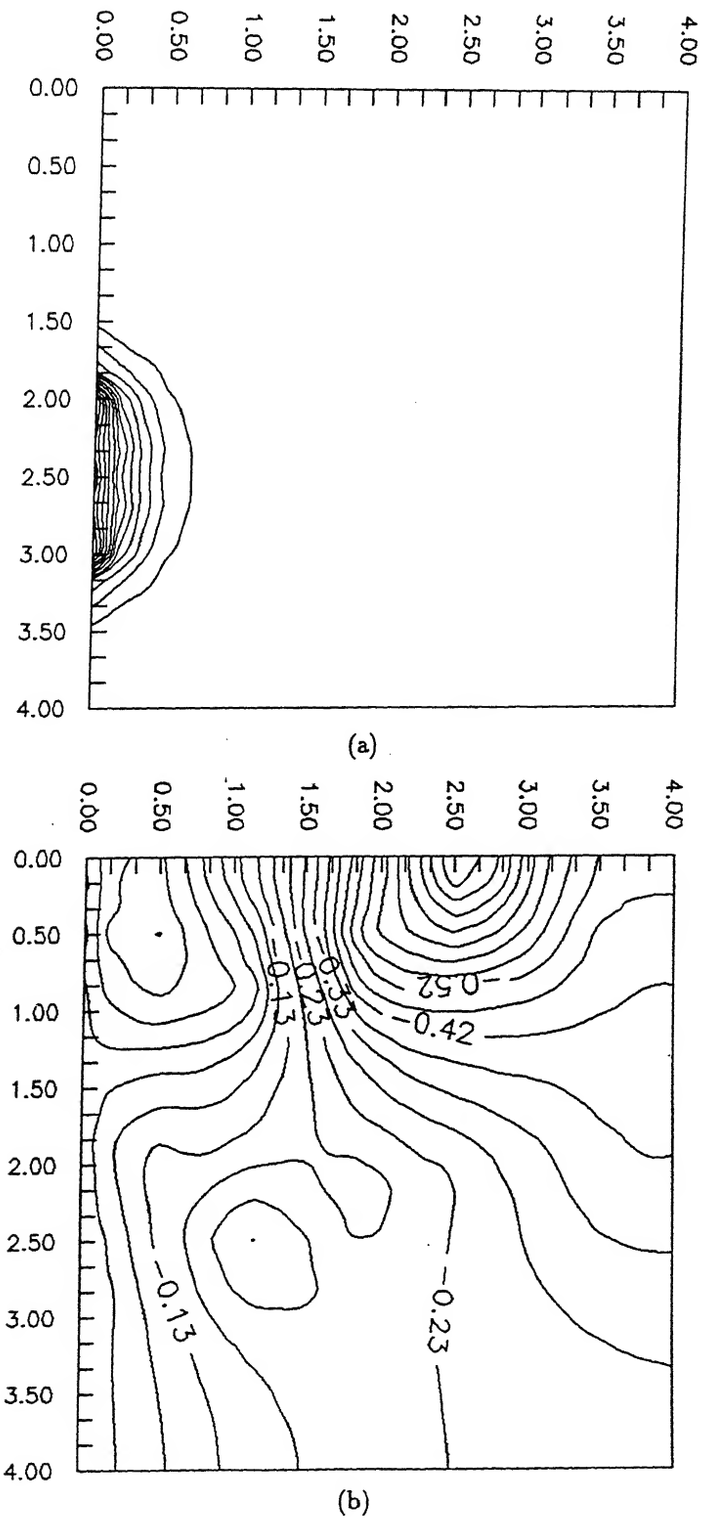

Figure 4.32: (a) Isotherms and (b) Streamlines at Plane 7 : Ra=10^5 and Pr=0.71

Chapter 5

Conclusions

Problems of buoyancy driven fluid flows and heat transfer in rectangular enclosures as well as in a channel section between the vertical fin arrays have been successfully solved using the Spectral Element Method. A semi-implicit formulation is used to solve the coupled heat transfer and fluid flow problems. Although the formulation of the problems is semi-implicit, the time stepping is chosen rather conservatively. The time step depends on the type of problem chosen.

For the case of flow in a differentially heated cavity, excellent agreement has been obtained between the results of earlier investigations and the present computation. For the problem of buoyancy driven cavity with discrete heat sources on a side wall, the results of the present computation agree well with those of Ho and Chang [20]. The problem addresses the cooling of integrated circuit packages for computers and other electronic applications.

Finally some useful predictions are done for buoyancy driven flow in a vertical channel formed by fin arrays. The magnitude and surface distribution of the heat transfer coefficient are predicted. The results are compared with the previous numerical results based on simplifying assumptions.

Bibliography

[1] C. Canuto, M. Y. Hussaini, A. Quarteroni, and T. A. Zang, "*Spectral Methods in Fluid Dynamics*", Springer-Verlag, Heidelberg, 1988.

[2] A. T. Patera, A Spectral Element Method for Fluid Dynamics: Laminar Flow in a Channel Expansion, *J. Comput. Phys.* , vol. 54, pp. 468-488, 1984.

[3] K. Z. Korczak and A. T. Patera, An Isoparametric Spectral Element Method for Solution of Navier-Stokes Equations in Complex Geometry, *J. Comput. Phys.*, vol. 62, pp. 361-382, 1986.

[4] A. Karageorghis and T. N. Phillips, Chebyshev Spectral Collocation Methods for Laminar Flow through a Channel Contraction, *J. Comput. Phys.*, vol. 84, pp.114-133, 1989.

[5] A. Karageorghis and T. N. Phillips, Spectral Collocation Methods for Stokes Flow in Contraction Geometries and Unbounded Domains, *J. Comput. Phys.* , vol. 80, pp. 314-330, 1989.

[6] Hong Ma, A Spectral Element Basin Model for the Shallow Water Equations, *J. Comput. Phys.*, vol. 109, pp. 133-149, 1993.

[7] A. Cloot and J. A. C. Weideman, An Adaptive Algorithm for Spectral Computations on Unbounded Domains, *J. Comput. Phys.*, vol. 102, pp. 398-406, 1992.

[8] Hoa D. Nguyen and Jacob N. Chung, A Chebyshev-Legendre Spectral Method for the Transient Solutions of Flow past a Solid Sphere, *J. Comput. Phys.* vol. 104, pp. 303-312, 1993.

[9] W. Cai, H. C. Lee, and H. S. Oh, Coupling of Spectral Methods and the p-version of the Finite Element Method for Elliptic Boundary Value Problems Containig Singularities, *J. Comput. Phys.* vol. 108, pp. 314-326, 1993.

[10] R. Peyret and T. Taylor, "*Computational Methods for Fluid Flow*", Springer-Verlag, Heidelberg, 1986.

[11] R. K. Datta, Implementation of The Two-Dimensional Helmholtz Solver, *M. Tech Thesis*, Dept. of Mech. Engg. I.I.T., Kanpur-208016, India, 1993,

[12] C. S. Tan, A Multi-domain Spectral Computation of Three -dimensional Laminar Horseshoe Vortex Flow Using Incompressible N-S Equations, *J. Comput. Phys.* ,vol. 85, pp. 130-158, 1989.

[13] N. K. Ghaddar, G. E. Karniadakis, and A. T. Patera, A Conservative Isoparametric Spectral Element Method for Forced Convection; Application to Fully Developed flow in Periodic Geometries, *Numer. Heat Transfer*, vol. 9, pp. 277-300, 1986.

[14] G. S. Shiralkar and C. L. Tien, A Numerical Study of Natural Convection in Shallow Cavities, *Journal of Heat Transfer (ASME)*, vol. 103, pp. 226-231, 1981.

[15] T. N. Philips, Natural Convection in an Enclosed Cavity, *J. Comput. Phys.* , vol. 34, pp. 365-381, 1984.

[16] K. Kublbeck, G. P. Merker and J. Straub, Advanced Numerical Computation of Two-Dimensional Time-Dependent Free Convection in Cavities, *Int. J. Heat Mass Transfer*, vol. 23, pp. 203-217, 1980.

[17] B. Ramaswamy, Finite Element Solution for Advection and Natural Convection Flows, *Computers & Fluids*, vol. 16, pp. 349-388, 1988.

[18] Wang Pu, Spline Method of Fractional Steps in Numerical Model of Unsteady Natural Convection Flow at High Rayleigh Numbers, *Numer. Heat Transfer*, vol. 11, pp. 95-108, 1987.

[19] J. Szekely and M. R. Todd, Natural Convection in a Rectangular Cavity Transient Behaviour and Two Phase Systems in Laminar Flow, *Int. J. Heat Mass Transfer*, vol. 14, pp. 467-482, 1971.

[20] C. J. Ho and J. Y. Chang, A Study of Natural Convection Heat Transfer in a Vertical Rectangular Enclosure with Two-Dimensional Discrete Heating: Effect of Aspect Ratio, *Int. J. Heat Mass Transfer*, vol. 37, pp. 917-925, 1994.

[21] S. Chakraborty, S. P. Sengupta and G. Biswas, Fluid Flow and Heat Transfer in a Laminar Radial Impinging Jet, *Int. J. Num. Meth. Heat Fluid Flow*, vol. 4, pp. 173-185, 1994.

[22] S. P. Sukhatme and N. H. Saikhedkar, Natural Convection Heat Transfer from Rectangular Cross-sectioned Vertical Fin Arrays, Journal of Thermal Engineering, vol. 1, pp. 125-132, 1980.

[23] M. A. I. Shalaby, U. N. Gaitonde and S. P. Sukhatme, Natural Convection Heat Transfer from Rectangular Vertical Fin Arrays, *Indian Journal of Technology*, vol. 22, pp. 321-327, 1984.